SCIENTIA ET TECHNICA

ISSN 0122-1701 - ISSN-E 2344-7214

La revista Scientia et Technica tiene inscripción vigente en la Sección de Registro de Propiedad Intelectual y Publicaciones del Ministerio de Gobierno de la República de Colombia, mediante Resolución 131 de marzo de 1995, Publicación aceptada en el Índice Nacional de Publicaciones Seriadas de Minciencia, Publindex en categoría B hasta el 31 de diciembre de 2021, Publicación asociada a la Red de Revistas Científicas de América Latina y El Caribe, España y Portugal (Redalyc), Vinculados a DIALNET, Centro de Información Tecnológica CIT., EBSCO-Academic Search Complete.

VOL 30 N°2

ABRIL - JUNIO DE 2025

Universidad Tecnológica de Pereira

Revista Scientia et Technica

Vol. 30, Núm.01 (enero-marzo) de 2025

https://revistas.utp.edu.co/index.php/revistaciencia/index

Contacto: scientia@utp.edu.co

DOI: https://doi.org/10.22517/issn.2344-7214

ISSN Electrónico (2344-7214)

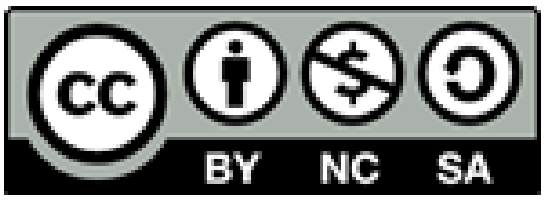

Pares evaluadores en este número

Jose Ricardo Bermudez Santaella
Michael Daniel Giraldo Galindo
Miguel Antonio Ojeda Enriquez
Julio Sanchéz Rendón
Raul Andres Becerra Arciniegas

Contenido

Scientia et Technica Año XXIX, Vol. 30, No. 02, abril-junio de 2025. Universidad Tecnológica de Pereira. ISSN 0122-1701 y ISSN-e: 2344-7214
DOI: 10.22517/23447214.25891

Editorial

La revisión científica como acto formativo y garante del conocimiento

En la de publicación científica, el revisor tiene un lugar esencial y, a la vez, discretamente invisible. Sus funciones son éticas académicas, éticas y formativas. Serlo no significa ejercer un juicio autoritario ni redactar una sentencia, más bien implica una gran responsabilidad con la comunidad académica que ha reconocido sus méritos. Pese a ello, la mayoría de las veces se realiza esta labor sin conciencia plena del impacto que la evaluación puede ejercer sobre una trayectoria investigativa o incluso sobre una línea de trabajo.

Más allá del juicio, un buen par evaluador es un lector objetivo, crítico, cuidadoso y comprometido que se identifica como un conocedor del tema. No basta con identificar errores o emitir recomendaciones generales. Su dictamen debe contribuir con base en criterios técnicos sólidos, a la mejora del manuscrito conservando siempre profundo respeto por los autores y el tema tratado. Por lo anterior, la revisión debe ser útil para el autor y para el editor, actuando como una oportunidad más mejoramiento de un manuscrito en desarrollo con oportunidad de publicación. Como señala el Committee on Publication Ethics (COPE), los revisores deben "valorar los méritos del artículo con objetividad, sin prejuicios personales ni consideraciones de nacionalidad, género, religión o afiliación institucional" [1].

Criterios esenciales para una revisión científica rigurosa

La evaluación por pares constituye un componente esencial del proceso editorial académico, ya que garantiza la calidad, originalidad y pertinencia de los manuscritos antes de su publicación. Para que esta labor cumpla su propósito de manera efectiva, debe tenerse una serie de atributos fundamentales que aseguren un aporte sustancial al mejoramiento del trabajo. Estos principios, reconocidos ampliamente por editoriales como Elsevier [2]–[4], constituyen los pilares de una revisión rigurosa, útil y profesional. A continuación, se detallan los aspectos clave que debe reunir un proceso de revisión científica de calidad:

1. **Dominio del tema:** El revisor debe contar con formación y experiencia comprobada en el área específica del manuscrito. La mayoría de las revistas selecciona a sus evaluadores de bases reconocidas, como Publindex (Colombia), o entre los autores citados en el estado del arte. Es poco probable que se asigne un manuscrito a alguien sin trayectoria investigativa en el campo, lo que convierte esta labor en un reconocimiento a la carrera académica del evaluador y, en muchos casos, en un motivo de orgullo profesional.
2. **Análisis completo:** Una revisión no debe limitarse a una lectura superficial o meramente formal. Se espera que el evaluador analice de manera integral la estructura, la metodología y los aportes del manuscrito. Si bien la calidad lingüística, la ortografía y la presentación gráfica son importantes, el verdadero valor de la revisión radica en su capacidad para valorar la coherencia científica, la validez del método y la relevancia de los resultados.
3. **Crítica constructiva:** Señalar deficiencias es parte de la función del evaluador, pero siempre debe hacerse con respeto y con el propósito de mejorar el trabajo. Una buena revisión no implica necesariamente aceptar el manuscrito, sino orientar al autor mediante observaciones claras y sugerencias fundamentadas sobre cómo fortalecer su propuesta.
4. **Claridad estructural:** Las observaciones deben presentarse de forma organizada, precisa y sin ambigüedades. Por esta razón, muchas revistas proveen listas de verificación o pautas estructuradas que orientan al revisor en aspectos formales, metodológicos y conceptuales, haciendo énfasis en la contribución científica del artículo.
5. **Ética editorial:** La confidencialidad, la honestidad intelectual y la ausencia de conflicto de intereses son principios inquebrantables. Un evaluador no debe divulgar, utilizar ni apropiarse del contenido del manuscrito en evaluación. Asimismo, debe actuar con profesionalismo incluso si el artículo aborda temas de su interés personal, reconociendo que el juicio científico debe prevalecer sobre los intereses individuales.
6. **Compromiso con los tiempos editoriales**: El cumplimiento de los plazos establecidos por la revista es esencial para asegurar la circulación oportuna del conocimiento científico. Si el evaluador no dispone del tiempo necesario para cumplir con esta responsabilidad, es preferible que rechace la invitación a revisar. La ciencia, en muchos casos, tiene un componente de obsolescencia, y las demoras innecesarias pueden afectar el impacto y la pertinencia de la publicación.

Como señala Elsevier en sus directrices, una revisión útil debe ser objetiva, específica y claramente redactada, proporcionando evidencia para sus recomendaciones [2]–[4]. En este sentido, la labor del revisor no solo valida el conocimiento, sino que también contribuye activamente a su fortalecimiento.

Conductas inaceptables en el proceso de revisión por pares

Por otro lado, la revisión por pares no debe transformarse en un juicio autoritario ni convertirse en un canal para expresar frustraciones, imponer ideas o desestimar trabajos ajenos sin argumentos sólidos. Cuando un revisor incurre en conductas inapropiadas se afecta también la credibilidad del proceso editorial. A continuación, se describen algunas de las prácticas inaceptables, con el respaldo de las principales directrices editoriales reconocidas:

1. **Emitir juicios despectivos, sarcásticos o irónicos**: siempre los comentarios deben ser respetuosos y profesionales. En estos casos, los editores están facultados para eliminar cualquier contenido ofensivo o personal [5] o, inclusive, no considerar la evaluación.
2. **Solicitar citas propias sin justificación técnica clara**: Se recomienda que los revisores no sugieran la inclusión de referencias personales a menos que sean claramente relevantes para el contenido del manuscrito [6].
3. **Rechazar o aceptar un artículo sin lectura detenida**: las editoriales establecen que los revisores deben realizar una evaluación completa e imparcial, con base en los méritos científicos del trabajo y no en impresiones [7].
4. **Hacer comentarios vagos o con base en preferencias personales**: Las editoriales científicas más destacadas enfatizan que los informes deben estar fundamentados en criterios objetivos, evitando juicios arbitrarios o imprecisos [5], [7].
5. **Influir en decisiones editoriales con sesgos ideológicos o geográficos**: Se subraya que la evaluación debe centrarse en el contenido científico del artículo, sin prejuicios relacionados con la nacionalidad, afiliación institucional o enfoque temático del autor [5].
6. **Uso inadecuado de Inteligencia artificial**: Las herramientas de inteligencia artificial en línea para analizar manuscritos en proceso de revisión representa una violación potencial de la confidencialidad del proceso editorial. Según las directrices de COPE, los revisores están obligados a mantener la confidencialidad de todo el material recibido y no deben compartirlo ni utilizarlo fuera del contexto de la evaluación [1]. En general, las editoriales enfatizan que los manuscritos son documentos confidenciales y que cualquier análisis automatizado debe contar con la autorización explícita de la revista, dado que puede comprometer tanto la integridad del contenido como la introducción de sesgos en el juicio evaluador [2]. En algunos casos, podría considerarse el uso de herramientas locales que pueden mantener la confidencialidad, lo que puede apoyar la revisión gramatical y otros aspectos no profundos, pero que son, de igual manera, relevantes de ser considerados.

Evitar estas prácticas protege la integridad del arbitraje y refuerza la confianza en la revisión por pares como mecanismo legítimo de validación científica. La excelencia en la revisión depende del conocimiento técnico y del compromiso ético, la equidad y la responsabilidad profesional.

En la experiencia editorial de la revista Scientia et Technica, se han recibido dictámenes que, aunque formulan algunas observaciones técnicas válidas, lo hacen con un lenguaje ofensivo, poco respetuoso o desproporcionadamente negativo. En tales casos, el comité editorial actúa con rigor: modera el tono del dictamen, reconsidera su pertinencia e incluso puede descartarlo si evidencia una falta de profesionalismo explícito. Se han detectado casos de evaluaciones marcadas por sesgos personales, institucionales o regionales, que afectan gravemente la imparcialidad del proceso. Incluso cuando el fondo puede ser rescatable, la forma en que se comunican las críticas puede anular cualquier beneficio. Ser celoso profesionalmente no significa ser hostil ni altivo; al contrario, es actuar con rigor y respeto, con conciencia del impacto que tiene cada observación sobre la trayectoria científica del autor.

El proceso de revisión no puede desligarse de las orientaciones editoriales. Todo revisor debe conocer y respetar las políticas específicas de la revista, así como el formato de evaluación proporcionado, si existe. Estos elementos orientan la estructura de la evaluación al mismo tiempo que aseguran la equidad del proceso, garantizando que todos los autores sean evaluados bajo criterios comunes y transparentes. Algunas revistas, como Scientia et Technica, establecen claramente qué dimensiones deben evaluarse: originalidad, rigor metodológico, solidez argumentativa, redacción académica, adecuación bibliográfica, entre otros aspectos.

Aspectos básicos que debe considerar un par evaluador

La calidad de la revisión por pares depende en gran medida de la profundidad y enfoque con que se examina el manuscrito. Aunque muchas revistas científicas proporcionan formularios o listas de verificación específicas, en aquellos casos donde no se establece una estructura formal, se recomienda que el revisor contemple, como mínimo, los siguientes aspectos fundamentales que reflejan el estándar internacional en la evaluación académica [8]:

1. **Pertinencia del tema y claridad del objetivo**: El artículo debe abordar un problema relevante dentro del campo de la revista y establecer con precisión su propósito. Como señala Springer, un buen manuscrito debe dejar claro qué busca responder y por qué es importante [9].
2. **Originalidad y aporte al estado del arte**: Es fundamental verificar si el trabajo presenta una contribución novedosa y si contextualiza adecuadamente su enfoque frente a la literatura existente [9].
3. **Rigor metodológico**: La metodología debe ser apropiada, reproducible y suficientemente detallada para garantizar la validez del estudio. IEEE resalta que el método debe permitir evaluar la solidez del análisis y la replicabilidad del experimento [8].
4. **Coherencia lógica y estructura argumentativa**: El texto debe mostrar una secuencia lógica entre la hipótesis, el desarrollo teórico, la evidencia empírica y las conclusiones. Taylor & Francis enfatiza la necesidad de una estructura clara y razonamiento sólido [10].
5. **Calidad de la redacción académica**: La claridad, precisión y estilo académico del lenguaje empleado impactan directamente en la comprensión del trabajo. Springer sugiere que el lenguaje debe ser profesional y sin ambigüedades [9].

6. **Uso adecuado y actualizado de referencias**: Las citas deben ser pertinentes, actuales y reflejar el dominio del tema. También es importante que se usen adecuadamente para respaldar afirmaciones clave [10].
7. **Resultados y análisis**: Deben presentarse de forma clara, con interpretaciones coherentes y análisis consistentes. IEEE recomienda que los resultados estén vinculados explícitamente a los objetivos y preguntas de investigación [8].
8. **Conclusiones justificadas**: Estas deben obtenerse directamente de los resultados, sin extrapolaciones indebidas. Es deseable que incluyan limitaciones del estudio y posibles líneas futuras de investigación [9].

Además, cuando se trata de un artículo derivado de investigación científica, es altamente recomendable que el evaluador verifique si el manuscrito se ajusta al formato IMRaD (Introducción, Métodos, Resultados y Discusión), el cual constituye un estándar internacional en la presentación estructurada de investigaciones [11]. Este formato facilita la comprensión del trabajo y la revisión objetiva:

- **Introducción**: Expone el contexto, la motivación y el objetivo del estudio.
- **Métodos**: Detalla el diseño experimental, técnicas y procedimientos usados para obtener los datos, permitiendo la reproducibilidad del trabajo.
- **Resultados**: Presenta los hallazgos de forma clara y ordenada, sin interpretaciones personales.
- **Discusión**: Interpreta los resultados, los contrasta con la literatura y establece su relevancia, limitaciones y posibles aplicaciones.

Al adoptar estos criterios mínimos se eleva la calidad de la revisión y contribuye a mantener la integridad y el rigor de la publicación científica. Estos principios están alineados con las guías éticas y técnicas de las principales editoriales internacionales.

Ser un buen revisor es un privilegio; es una función esencial en la construcción del conocimiento científico a un nivel cercano de quien lo genera [12]. Una revisión rigurosa y respetuosa contribuye al desarrollo de mejores investigaciones, al fortalecimiento de las revistas y al crecimiento de toda la comunidad académica. Hacerlo bien también forma al revisor: lo obliga a leer críticamente, a contrastar sus propios criterios y a mantenerse actualizado. En ese espíritu, Scientia et Technica invita a sus revisores a asumir esta tarea con ética, generosidad intelectual y un compromiso inquebrantable con el saber.

Referencias.

[1] Committee on Publication Ethics (COPE), "Ethical Guidelines for Peer Reviewers," 2017. [Online]. Available: https://publicationethics.org/guidance/guidelines-new/ethical-guidelines-peer-reviewers

[2] Elsevier, "How to review a manuscript," Elsevier Reviewer Hub. [Online]. Available: https://www.elsevier.com/reviewers/how-to-review

[3] Elsevier, "Guide for Reviewers – Ophthalmology," Elsevier Health. [Online]. Available: https://els-jbs-prod-cdn.jbs.elsevierhealth.com/pb/assets/raw/Health%20Advance/journals/ophtha/guideRev.pdf

[4] Elsevier, "Reviewer Guidelines," Elsevier Researcher Academy, 2022. [Online]. Available: https://www.elsevier.com/reviewers

[5] Springer Nature, "Peer Review Policy, Process and Guidance." [Online]. Available: https://www.springer.com/gp/editorial-policies/peer-review-policy-process

[6] J. Smith, "Best Practices in Peer Review," *Journal of Scholarly Publishing*, vol. 49, no. 2, pp. 123–135, 2018.

[7] M. Resnik and D. Elmore, "Ensuring Research Integrity through Peer Review," *Science and Engineering Ethics*, vol. 22, pp. 169–188, 2016.

[8] IEEE, "IEEE Journals and Magazines Reviewer Guidelines," Updated 3 April 2024. [Online]. Available: https://ieeeauthorcenter.ieee.org/wp-content/uploads/ieee-reviewer-guidelines.pdf

[9] Springer Nature, "Author and Reviewer Guidelines." [Online]. Available: https://www.springernature.com/gp/authors/research-data-policy/data-policy-types/research-data-policy-type-1

[10] Taylor & Francis, "The ethics of peer review," Taylor & Francis Reviewer Resources. [Online]. Available: https://editorresources.taylorandfrancis.com/managing-peer-review-process/the-ethics-of-peer-review

[11] International Committee of Medical Journal Editors (ICMJE), "Recommendations for the Conduct, Reporting, Editing, and Publication of Scholarly Work in Medical Journals." [Online]. Available: https://www.icmje.org/recommendations

[12] J. A. Cortes Osorio, "The privilege of becoming a scientific peer reviewer," *Scientia Et Technica*, vol. 24, no. 1, art. 5, Mar. 2019. doi: 10.22517/23447214.21311.

Autor

PhD. Jimy Alexander Cortes Osorio
Docente Titular Departamento de Física
Editor jefe -Revista Scientia et Technica
Grupo Investigación Robótica Aplicada
Línea: Computer Vision and Machine Learning
Investigador Senior Reconocido por MINCIENCIAS
Universidad Tecnológica de Pereira
ORCID: https://orcid.org/0000-0002-0413-807X

Analysis of the conversion efficiency and THD of DC/AC converters used in off-grid photovoltaic generation system

Análisis de la eficiencia de conversión y THD de convertidores DC/AC empleados en un sistema de generación fotovoltaica aislado de la red

J. Fernández Zorro; N. J. Rodríguez Ballesteros; E. W. Suarez Chaparro

DOI: https://doi.org/10.22517/23447214.24807
Scientific and technological research paper

Abstract— This article presents an experimental analysis of the conversion efficiency and total harmonic distortion (THD) of two DC/AC converter prototypes designed for off-grid photovoltaic generation systems (OPGS). The objective is to determine the influence of two controllable factors; the DC input voltage and the percentage of nominal load at the output, on the converters' performance. The prototypes, based on unipolar SPWM modulation, were implemented using simulation software, and tested under a factorial experimental design. The study applied statistical methods, including ANOVA, to analyze the effect of each factor and their interaction on the two response variables: efficiency and THD. Results showed that for the first prototype, efficiency is independent of DC input voltage but dependent on load, while THD is influenced by both factors. In the second prototype, both efficiency and THD are affected by variations in both factors, with THD showing instability due to LC network resonance. The comparison reveals that locating the LC filter after the transformer slightly improves THD but reduces efficiency due to increased harmonic losses. These findings are relevant for optimizing inverter design in isolated PV systems.

Index Terms —Efficiency; Experimental d esign; Inverter; Photovoltaic system; Total harmonic distortion.

***Resumen*— Este artículo presenta un análisis experimental de la eficiencia de conversión y la distorsión armónica total (THD) de dos prototipos de convertidores DC/AC diseñados para sistemas de generación fotovoltaica aislados de la red (OPGS). El objetivo es determinar la influencia de dos factores controlables, el voltaje DC de entrada y el porcentaje de carga nominal conectada a la salida sobre el desempeño de los convertidores. Los prototipos, basados en modulación SPWM unipolar, fueron implementados mediante software de simulación y evaluados bajo un diseño experimental factorial. Se aplicaron métodos estadísticos, incluyendo ANOVA, para analizar el efecto de cada factor y su interacción sobre las dos variables de respuesta: eficiencia y THD. Los resultados mostraron que, para el primer prototipo, la eficiencia es independiente del voltaje DC de entrada pero dependiente de la carga, mientras que la THD está influenciada por ambos factores. En el segundo prototipo, tanto la eficiencia como la THD se ven afectadas por las variaciones de ambos factores, y la THD presenta inestabilidad debido a la resonancia de la red LC. La comparación revela que ubicar el filtro LC después del transformador mejora ligeramente la THD, pero reduce la eficiencia debido a mayores pérdidas por armónicos. Estos hallazgos son relevantes para optimizar el diseño de inversores en sistemas fotovoltaicos aislados.**

Palabras clave — Diseño experimental; Distorsión armónica total; Eficiencia; Inversor; Sistema fotovoltaico.

I. Introduction

DC/AC converters, also called inverters, are subsystems commonly used to convert direct current (DC) into alternating current (AC), with applications in motor control, energy conversion, and renewable energy systems [1]. Photovoltaic (PV) generation systems, whether grid-connected or off-grid, rely on these converters to adapt solar energy to the requirements of electrical loads and to enable efficient energy management [2]. Due to increasing global energy demand and the environmental impact of traditional power generation methods, photovoltaic systems have become more relevant. Since inverters are central to these systems, it is essential to study their conversion efficiency and the quality of the output power they deliver [3].

Recent studies have analyzed the performance of different inverter topologies, considering aspects such as switching techniques, filter configurations, and control strategies. For instance, transformer-less designs and LC filter placement have shown significant effects on total harmonic distortion (THD) and energy losses [3][4]. Some authors have explored the influence of DC input voltage and load variation on inverter performance, highlighting the role of design parameters on harmonic behavior and efficiency [5]. In particular, Rampinelli et al. [7] proposed mathematical models that relate inverter efficiency to input voltage and output power, demonstrating

This manuscript was submitted on July 30, 2024. Accepted on June 16, 2025, and published on June 30, 2025.

Elkin Wbeimar Suarez is affiliated with Future Solutions Development S.A.S., OTTIS HARDWARE Department, Sogamoso, Colombia (e-mail: elkinsuarezews@gmail.com).

Johan Andrés Fernández is affiliated with Future Solutions Development S.A.S., OTTIS HARDWARE Department, Sogamoso, Colombia (e-mail: andresjfz10@gmail.com).

Nairo Julián Rodríguez is affiliated with SENA, SENNOVA Research Group, Sogamoso, Colombia (e-mail: njrodriguez43@misena.edu.co)

good accuracy for grid-connected PV systems. Similarly, Farfán and Massen [15] evaluated two mathematical approaches to model how variations in input voltage affect conversion efficiency, supporting the importance of this variable in experimental analysis. Likewise, Gallego-Gómez et al. [8] analyzed conduction losses in SPWM-modulated inverters, providing a mathematical formulation that links internal power losses to efficiency degradation. Similarly, Lázaro Campo [12] analyzed the performance of photovoltaic installations in relation to inverter operation and final energy yield, highlighting the importance of matching design parameters to specific environmental conditions. Moreover, comprehensive reviews have compared the behavior of single-phase inverters in photovoltaic applications, providing insights for optimizing topology selection based on THD limits and energy quality standards [1][2]. Additionally, Beltrán Telles et al. [9] carried out an experimental evaluation of H-bridge inverters using SPWM, demonstrating that harmonic distortion and waveform quality are significantly affected by switching strategies and load variations—an aspect that closely aligns with the objectives of this study.

Beyond mathematical modeling, experimental analysis remains a fundamental tool for understanding system behavior under controlled conditions. An experiment involves varying input parameters to observe their influence on selected response variables. However, many experimental efforts rely on trial-and-error methods, which often lack the structure required for drawing reliable and reproducible conclusions. A more rigorous and effective approach involves the use of Experimental Design [6][11], which offers a statistically supported framework for identifying and quantifying the effects of key factors on system performance.

This research applies an Experimental Design methodology to analyze the conversion efficiency and THD of two unipolar SPWM DC/AC converter prototypes implemented via simulation software. Similar approaches have been used in studies of converter performance for UPS applications, where simulation environments enable detailed control and comparison of circuit configurations [14]. The study considers the DC input voltage and the percentage of nominal load at the output as influencing factors. Based on these, null and alternative hypotheses are formulated for each response variable and evaluated through ANOVA statistical analysis..

This paper is organized as follows: Section II presents the design and definition of factors; Section III details the simulation methodology; Section IV discusses the results; and finally, Section V provides the main conclusions.

II. CONSTRUCTION OF THE EXPERIMENTAL DESIGN

The Experimental Design is structured under the guidelines shown in Fig. 1.

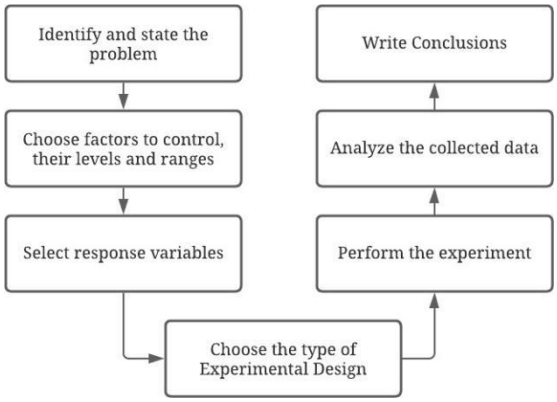

Fig. 1. General guidelines for designing an experiment [7].

A. Identify and state the problem

The problem consists in determining the influence of the DC voltage applied to the inverter input and the percentage of nominal load connected to its output, on the conversion efficiency and the total harmonic distortion. For this, it is essential to determine the set of tests to be applied, the way to apply them, and the way to collect and analyze the data. Fig. 2, presents the DC/AC converter under investigation, which belongs to an OPGS and uses unipolar SPWM modulation.

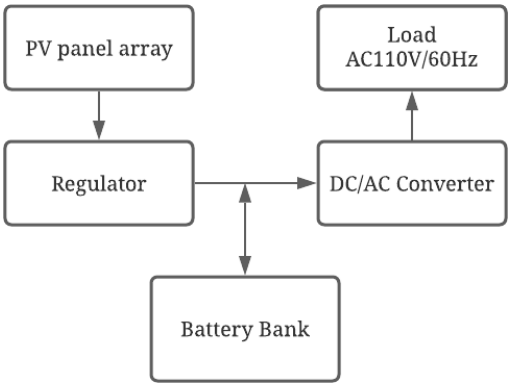

Fig. 2. Block diagram of an OPGS. Source: own

B. Choose factors to control, their levels and ranges

Different types of variables or factors intervene in every process, such as those shown in Fig. 3. The response variables generally coincide with the output variables of the system and are used to measure its performance and evaluate the effect of the experiment. The controllable factors are the input variables of the process, over which there is control, for this there must be a mechanism that allows the experimenter to change or fix their levels. The uncontrollable factors, also called noise, correspond to those input variables over which there is no control, such as physical, environmental or inherent phenomena to the process and that appear randomly, affecting its behavior. [8].

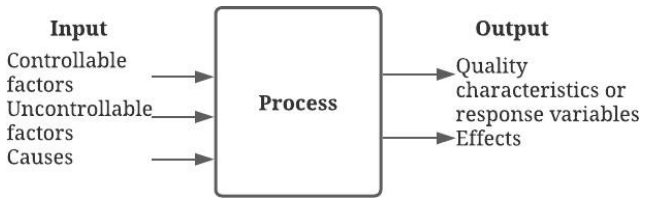

Fig. 3. Variables involved in a process. Based on [8].

Table I shows the most relevant considerations when sizing an OPGS. Taking into account that the DC / AC converter (inverter) is the study center of this research, aspects such as the voltage of the battery bank, the nominal power, the efficiency, the THD and the type of load to be fed, are of great interest.

In accordance with [9], one of the most important parameters and that best represents the operation of a PV inverter is its efficiency curve. Efficiency (η_{inv}), is the ratio between the energy delivered to a load and the energy required by the inverter. As the inverter is a central block in an OPGS, the efficiency curve provides decisive information for its sizing.

THD is an important variable in electricity generation systems, since it indicates the quality of the energy that is being delivered to the load. The harmonics produced by PV inverters can generate problems within an OPGS, reducing the useful life of electronic devices, therefore, the study of harmonics from THD measurements is crucial [10].

Inverter's efficiency, lies according to operation point on it works. Depending of supplied rated power (Po_{AC}) and (V_{DC}), we obtains the efficiency that is calculated through (1), where F_p is the power factor, V_{rms} is the effective voltage of the inverter, I_{rms} is the effective current an I_{DC}, is the average current supplied for the DC source [9].

$$\eta_{inv} = \frac{Po_{AC}}{Pin_{DC}} = \frac{V_{rms} \cdot I_{rms} \cdot F_p}{V_{DC} \cdot I_{DC}} \quad (1)$$

On an inverter, the THD of the voltage wave (THD_V) and of the current wave (THD_i) can be analyzed, these parameters generally depend: of the type of inverter, of the filters used, of the linearity of the load and of the rated power supplied, and it is calculate using (2), whereV_1, is the effective value of the fundamental harmonic.

$$THD_V = \sqrt{\left(\frac{V_{rms}}{V_1}\right)^2 - 1} \quad (2)$$

Table II, shows a resume of the variables that interact on a DC/AC converter. Taking into account the information provided on the Fig. 3, it can be considered as controllable factors [11]: The DC voltage applied in the input, the load connected on the output and the type of load. As response variables, can be chosen: converter´s temperature, the conversion efficiency and the THD on the voltage wave of the output. Exist other no controllable variables as the electromagnetic noise, generated both by the converter and by external agents, and the climatic conditions.

For this research, the controllable factors chosen are: the DC voltage applied on the input of the inverter and load´s percentage connected on the output, considering for the analysis purely resistive loads. For the first factor, 6 levels are chosen and for the second 10 levels[3] [12]. On the other hand, no controllable factors are neglected, and the efficiency and THD of the voltage wave are considered as response variables.

C. Choose Experimental Design Type

There are many types of experimental designs to study different problems or situations, however, there are five aspects that influence when choosing one or the other, these are: the objective of the experiment, the number of factors to study, the number of levels that The effects to be investigated and the cost, time and desired precision are tested on each factor [8].

For this research a factorial type experimental design are choose, whose main characteristics are presented on Table III Table IV shows the levels assigned to the controllable factors. In the case of DC voltage, 6 voltage levels are proposed that are within the expected range for the most common battery banks. For the output load, 10 levels expressed as a percentage of the nominal power of the inverter under test were established.

Taking in account that are raised a experimental design with two controllable factors, we propose the next nulls hypotheses: $H0_1$: The efficiency conversion, as well as the THD are independents of DC voltage variation at input of the inverter. $H0_2$: The efficiency conversion, as well as the THD are

TABLE I
VARIABLES THAT INTERACT IN A DC/AC CONVERTER

Variable	Characteristic
Input DC Voltage (V)	Controllable Factors
Load connected to the output (% of nominal)	
Type of load R-L-C	
Converter Temperature (°C)	Response Variables
Conversion Efficiency(%)	
THD on output voltage (%)	
Electromagnetic noise	Non Controllable Variables
Climatic conditions	

Variables: DC = Direct Current; AC = Alternated Current; V = Voltage, η = Conversion Efficiency; THD = Total Harmonic Distortion ; °C = Celsius degrees, Load Types; R = Resistive; L = Inductive; C = Capacitive

TABLE II
CONSIDERATIONS WHEN SIZING AN OPGS

Variable	Characteristic
PV array	Morphology – Distribution – Angle of incidence– Distance to battery bank
Battery Bank	Technology – Backup time – Voltage – Connection
Commercial power grid	Availability – Voltage – Frecuency
Charge regulator	Availability – PWM – MPPT
Inverter	Type – Rated power – Temperature – Efficiency – THD
Load	Type (R, C, L) – Linear - Nonlinear - Consumption

Types of solar regulators: PWM = Pulse Width Modulation; MPPT = Maximum Power Point Tracker.

Most common types of loads: R = Resistive; C = Capacitive; L = Inductive; or combinations R-L-C.

Types of photovoltaic systems: GCPS = Grid Connected Photovoltaic System; OPS = Off – Grid Photovoltaic System.

independent of nominal load percentage connected at the inverter output.

$H0_3$: The efficiency conversion, as well as the THD are independent of DC voltage variation at the inverter input and the nominal load percentage connected at it's output.

The same way, the following alternative hypotheses are proposed:

HA_1: The efficiency conversion, as well as the THD are dependents of DC voltage variation at inverter input.

HA_2: The efficiency conversion, as well as the THD are dependent of nominal load percentage connected at the inverter output

HA_3: La eficiencia de conversión, así como la THD son dependientes de la variación del voltaje DC a la entrada del inversor y del porcentaje de carga nominal conectada a su salida.

In the next section the methodology employed for apply the proposed experimental design are presented.

III. METHODOLOGY FOR EXPERIMENTAL DESIGN EXECUTION

For this research are proposed two DC/AC converters that's use unipolar SPWM modulation, and that are designed for a nominal power of 2KVA. There block diagrams are shown in the Fig. 4 and Fig.5, respectively.

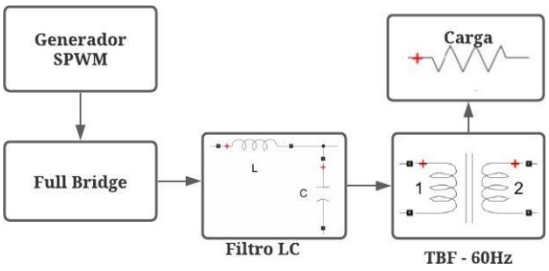

Fig. 4. Block diagram of first prototype DC/AC converter. Source: own

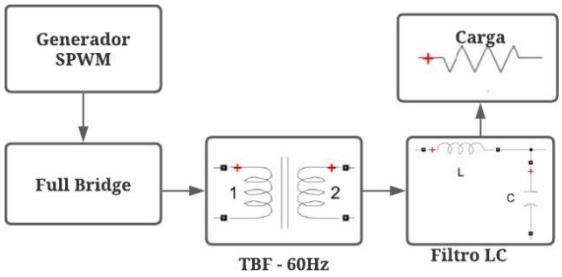

Fig. 5. Block diagram of second prototype DC/AC converter. Source: own

these prototypes were implemented using Matlab tool simulink simulation software[13], taking in account real parameters both in the Full bridge and in transformer , just with difference of LC network positioning [14][15]. with this prototypes ,are searching too , analyse the effect of LC network positioning, about their performance and energy quality.

For apply the experimental design ,we follow the scheme shown below, at Fig. 6.

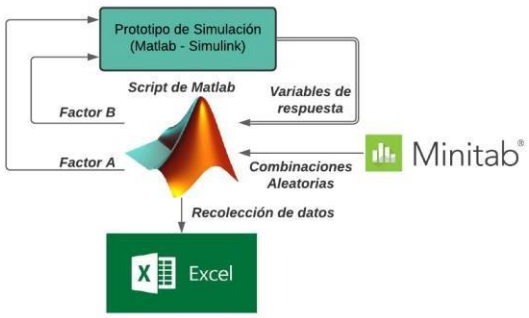

Fig. 6. Employed method for experimental design validation. Source:own

First, the 120 random runs were obtained using the Minitab software, taking into account that there are two controllable factors each with 6 and 10 levels and two repetitions during the experiment. Subsequently, a Matlab script was developed that works in conjunction with Simulink, modifying the values of each input factor according to the runs obtained in the previous step and collecting the data referring to efficiency and THD for each combination. Using the script, you get an array of data that is then exported and organized in a spreadsheet. Finally, an

TABLE III
CHARACTERISTICS OF PROPOSED EXPERIMENTAL DESIGN

Item	Value/Designation
Controllable Factors	2
Levels	6 y 10 respectively
Response Variable	2
Number of base runs	60
Specimens	2
Replicas	2
Randomness	Si
Number of total runs	240
Data to Collect	480

1. Controlable Factor: What can be varied during experiment
1. Level: Value that takes a controllable factor
2. Response Variable: what is case of study
3. Run: Combination of the factors
4. Specimens: Experimental unit

TABLE V
AVERAGE VALUES OF EFFICIENCY OF PROTOTYPE I

Controllable Factors		Factor A					
		22	23.6	25.2	26.8	28.4	30
Factor B	10	96.486	96.484	96.481	96.479	96.522	96.514
	20	96.728	96.692	96.691	96.69	96.688	96.719
	30	96.139	96.152	96.111	96.11	96.143	96.136
	40	95.371	95.346	95.382	95.38	95.376	95.343
	50	94.537	94.516	94.55	94.549	94.514	94.514
	60	93.681	93.664	93.697	93.696	93.692	93.662
	70	92.822	92.829	92.837	92.839	92.837	92.806
	80	91.963	91.968	91.978	91.949	91.978	91.977
	90	91.111	91.117	91.127	91.128	91.128	91.126
	100	90.271	90.263	90.285	90.29	90.263	90.289
Media: 93.97		Standard Deviation: 2.2				Variance: 4.84	

Controllable Factors: A = DC voltage at the input of the DC / AC Converter in volts (V); B = Percentage of nominal load connected to the output of the DC / AC Converter (%). Response variable: Conversion efficiency (%).

ANOVA analysis of variance is carried out and the main

effects and interaction graphs for each response variable and the normal probability graph are obtained. The results obtained are examined in detail in the following Section.

IV. Results

Table V, presents the average values of efficiency conversion of the first prototype, related to each of the runs or combinations that were applied during the experiment.

It can be seen that the average efficiency of this prototype is 93.97%, on the other hand, the standard deviation shows that the data is relatively homogeneous, since there is a separation from the mean. The Fig. 7, show the main effect of each of the factors about conversion efficiency of prototype I.

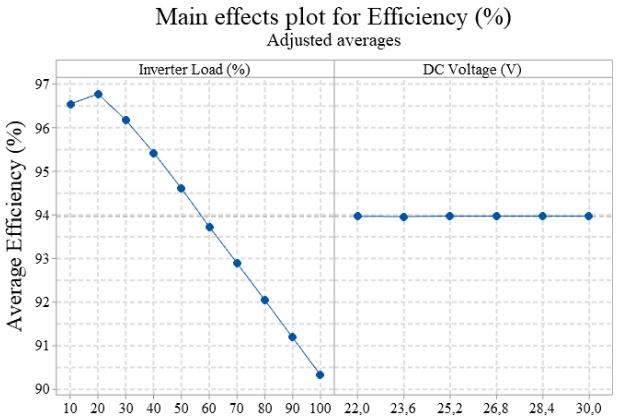

Fig. 7. Main effects graph for the efficiency of the prototype I. Source: own

At first glance, the efficiency compartment is not affected by variations in DC voltage, while the load percentage, if it has an effect on it, and is as mentioned in Section II, since, depending on the point inverter work, there is a different value for efficiency. Efficiency presents this behavior, because, as the load connected to the inverter increases, the current flowing through the switches, conductors and transformer also increases, the rising current increases the switching losses, due to the joule effect and due to the harmonics present, and according to the slope of the graph, these losses are not negligible. The Fig. 8, shown the effect produce for interaction of the both factors about efficiency.

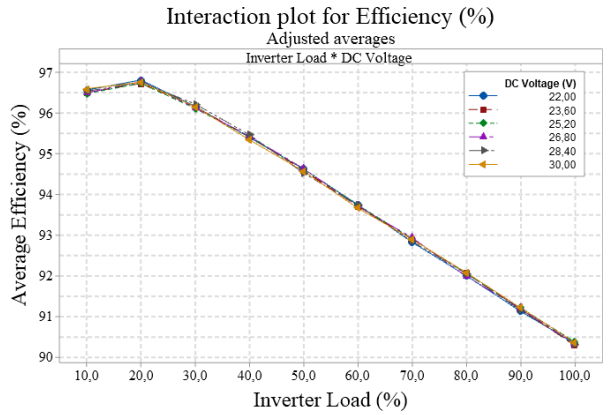

Fig. 8. Efficiency curves of prototype I. Source: own

In this graph , can be noticed clearly, that's DC voltage, doesn't have a significant effect over efficiency curve of the DC/AC converter, this can be explained from harmonics point of view, generated by used modulation required to obtain the sinusoidal equivalent waveform at the output. The harmonics generated in this type of systems, depends of many factors, among them, DC input voltage, tuning of LC network [14] [15], Switching frequency of full bridge, index amplitude modulation among others. The harmonics in general produce power losses in all elements that transport them, but for a OPGS, The power losses increase in the isolation transformer [16],For this reason, placing the LC filter behind the primary one prevents harmonics from being conducted by the transformer, for this reason, when the load remains constant and the DC voltage varies, the amplitude of the harmonics may change; however, they are not present at the transformer primary. As a result, the associated power losses are not reflected in the efficiency.

On the other hand, the interaction graph drives that´s for a nominal load of 100%, obtains a minimum efficiency of 90.5% approximately, whereas a load of 20%, the efficiency reaches it maximum value of 96.7% . the optimum operation point for this system its located around 50% of load, at this point we can extract the maximum power at a related good efficiency, this information is useful for implement OPGS, and analyse the different circumstances of operation of this important block.

Applying a statistical analysis ANOVA, can be determined with certainty, if the null hypotheses, exposed on the Section II are true and they must be accepted or, conversely, rejected. Table VI, shows the ANOVA for the efficiency of the prototype I.

Observing the values P, of each one of the factors of individual way of each of the factors individually and their interaction, It

TABLE VI
ANOVA FOR EFFICIENCY OF PROTOTYPE I

Source	DF	SS	MS	Valor F	Valor P
Inverter Load (%)	9	573.21	63.69	8246.5	0.000
DC Voltage (V)	5	0.002	0.0004	0.05	0.998
Inverter Load (%) * DC Voltage (V)	45	0.145	0.0032	0.42	0.999
Error	60	0.463	0.0077		
Total	119	573.82			

Statistical Terms: DF = Degrees of Freedom; SS = Sum of Squares; MS = Mean Square.

can be stated that the conversion efficiency of prototype I is dependent on the percentage of nominal load connected to its output and independent of the variation of the DC voltage applied to the input, and also independent of their interaction.

Fig. 9, presents the graphic of normal probability of obtained data for the efficiency. Considering a significance level of 0.05, it can be said that most of the data follow the adjusted distribution line and their behavior is normal.

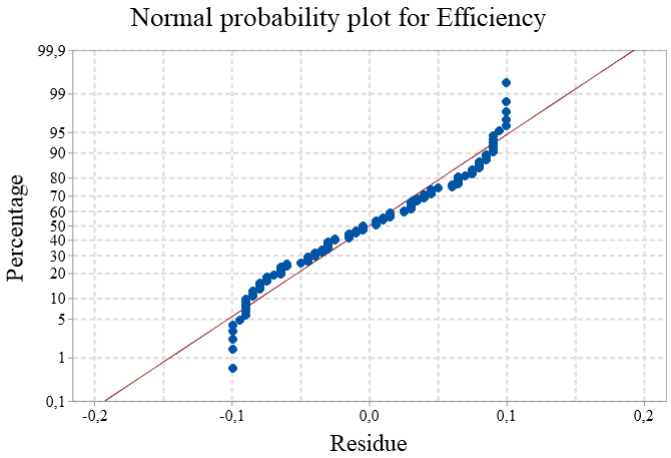

Fig. 9. Normal probability plot for the efficiency of the prototype I. Source: Own

Table VII, shows the average values of the THD of the voltage wave of prototype I. According to international standards such as IEEE519 or EN50160, the levels of total harmonic distortion must be less than 8%, for systems whose supply voltage is less than 1000V, in this way it is ensured that harmonics do not cause considerable damage. sensitive electronic devices. According to Table VII, the average THD for prototype I is 0.0461%, which is much less than 1%, as expected, when considering linear and purely resistive loads, however, this information serves to check the waveform output of prototype I.

Fig. 10, shows the response of the THD in front of individual variations of the controllable factors. According to this graphic, the THD depends both the DC voltage and the percentage of connected load. It is observed that for a load level between 10% and 90%, the THD varies proportionally with the load, this behavior is due to the resonant effect of the LC network, which causes an increase or decrease in harmonics, close to the resonant frequency.

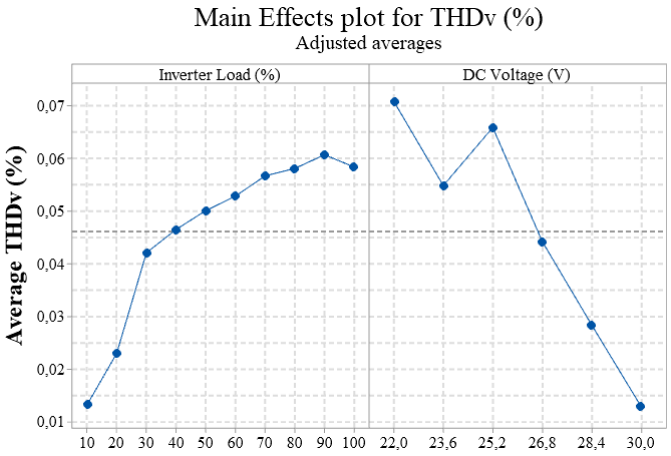

Fig. 10. Main effects plot for the THD of prototype I. Source: Own

Fig. 11 shows the interaction graph for the THD of the prototype I. With this graph, it can be clearly seen that the DC voltage has an influence on the THD response, since a different curve is obtained for each value. It is observed that the higher the DC voltage, the better the THD levels are obtained, this is due to the fact that the latter is inversely proportional to the amplitude of the fundamental harmonic, which is proportional to the input voltage [1].

TABLE VII
AVERAGE THD VALUES IN PROTOTYPE I

Controllable Factors		Factor A					
		22	23.6	25.2	26.8	28.4	30
Factor B	10	0.033	0.0012	0.01	0.001	0.004	0.001
	20	0.058	0.005	0.051	0.003	0.002	0.002
	30	0.059	0.064	0.055	0.028	0.016	0.003
	40	0.062	0.063	0.064	0.039	0.023	0.004
	50	0.069	0.06	0.069	0.045	0.021	0.005
	60	0.077	0.057	0.074	0.05	0.033	0.006
	70	0.078	0.063	0.079	0.056	0.034	0.007
	80	0.074	0.067	0.076	0.053	0.037	0.018
	90	0.078	0.065	0.075	0.064	0.042	0.016
	100	0.077	0.058	0.068	0.064	0.036	0.029
Media: 0.0461		Desviación Estándar: 0.027			Varianza: 0.00072		

Controllable Factors: A = DC voltage at the input of the DC / AC Converter in volts (V); B = Percentage of nominal load connected to the output of the DC / AC Converter (%).
Response variable: THD = Total Harmonic Distortion (%).

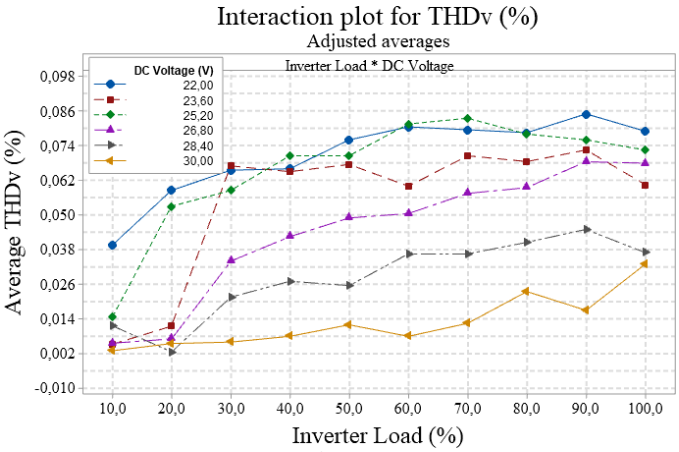

Fig. 11. THD Curves of prototype I. Source: Own

Table VIII, shows the ANOVA for THD of prototype I. Observing the P values, of each of the factors individually and their interaction, we can say, THD of prototype I, is dependent of nominal load percentage connected to output and dependent of variation of DC voltage applied to the input, but it also depends of their interaction.

TABLE VIII
THD ANOVA FOR PROTOTYPE I

Source	DF	SS	MS	Value F	Valor P
Inverter Load (%)	9	0.027	0.003	77.36	0.000
DC Voltage (V)	5	0.05	0.010	251.14	0.000
Inverter Load (%) * DC Voltage (V)	45	0.008	0.0002	4.68	0.000
Error	60	0.002	0.0000		
Total	119	0.088			

Statistical Terms: DF = Degrees of freedom; SS = Sum of squares; MS = Middle Square.

The Fig. 12, shows the normal probability graph of the THD values obtained during the experiment. According to the chosen level of significance, the experimental data behave according to the normal distribution line, however, there is a variability in the extremes that is common in this type of graph.

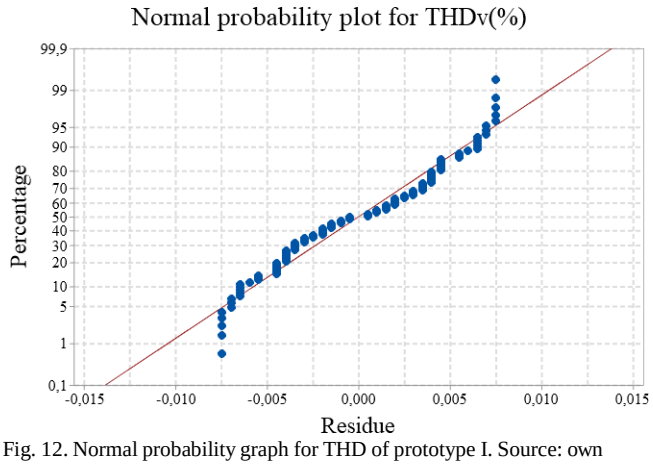

Fig. 12. Normal probability graph for THD of prototype I. Source: own

Next, the hypotheses raised in Section II are validated for this particular prototype.

The hypotheses $H0_1$, considers that's the conversion efficiency and the THD, are independents of the variation of DC voltage, although, the results shown that's efficiency are independent of DC input voltage , but THD are dependent, therefore must be rejected both hypotheses $H0_1$ and HA_1

The hypotheses $H0_2$, establish that's conversion efficiency and THD, are independents of nominal load percentage connected to the output inverter, however, the results shown both efficiency and THD , are depend of load percentage, by the arguments mentioned before the null hypotheses $H0_2$ are rejected but the alternate hypotheses are confirm HA_2

The hypotheses $H0_3$, assert efficiency conversion and THD, are independents of interaction between DC voltage and load percentage, however, the results allow assert efficiency is independent of there interaction, but THD is dependent. En this case, should be rejected both hypotheses, null $H0_3$and alternate HA_3.

Following, the same analysis is performed for conversion efficiency and THD of prototype II

The Table IX, shows the average values of conversion efficiency of prototype II, related with each combinations applied during experiment.

According to the results, the prototype II has an average efficiency of 93.73%, approximately 0.24% lower than that of prototype I. This is explained by the additional losses caused by high-frequency harmonics when the LC network is placed on the secondary side of the transformer. This observation is consistent with the findings of Gerardo and Miguel [10], who reported that post-transformer LC filters improve harmonic suppression but also introduce additional switching and conduction losses, slightly reducing overall efficiency. It is also observed that the data obtained are homogeneous, as in prototype I, according to the standard deviation..

TABLE IX
EFFICIENCY AVERAGE VALUES OF PROTOTYPE II

Controllable Factors		Factor A					
		22	23.6	25.2	26.8	28.4	30
Factor B	10	96.081	95.971	95.861	95.752	95.644	95.53
	20	96.486	96.43	96.374	96.317	96.262	96.20
	30	95.971	95.933	95.895	95.858	95.821	95.78
	40	95.231	95.207	95.179	95.151	95.122	95.09
	50	94.422	94.399	94.374	94.356	94.329	94.31
	60	93.58	93.56	93.535	93.523	93.504	93.48
	70	92.727	92.713	92.693	92.665	92.666	92.65
	80	91.872	91.86	91.846	91.814	91.816	91.80
	90	91.025	91.01	91.002	90.991	90.979	90.96
	100	90.186	90.179	90.169	90.159	90.147	90.13
Average: 93.73		Standard Deviation: 2.092			Variance: 4.38		

Controllable Factors: A = DC voltage at input DC/AC converter, volts (V);
B = Nominal load Percentage connected to DC/AC Converter (%).
Response Variable: Efficiency conversion (%).

The Fig. 13, shows the individual effect of every factor over conversion efficiency of prototype II.

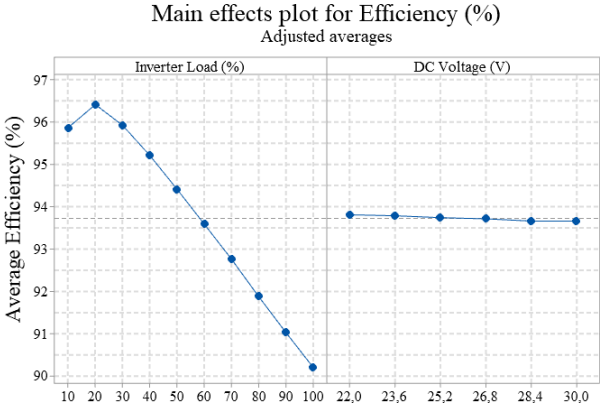

Fig. 13. Main effects plot for the efficiency of the prototype II. Source: Own

According to this graphic, both the DC voltage and the load percentage have an influence on the performance of the converter. In the case of efficiency, the same thing happens as in prototype I, since for each load value, there is a different efficiency. According to Fig. 13, the lowest efficiency is 90.13% and occurs when 100% of the load is connected, on the other hand, the maximum efficiency is 96.48% and like the prototype I, occurs for a 20% load. It is also observed that the DC voltage is inversely proportional to the efficiency, this is due to the fact that when the DC voltage increases, the mplitudes of the harmonics also increase, generating greater losses in the transformer.

Fig. 14, shows the effect that have the interaction of the two factors on the efficiency. According to this graphic, the effect of the interaction is remarkable for load levels lower than 50% , Despite of that, does not exist a big difference between one curve and the other, the largest difference is 0.5% and occurs for a 10% load, on the other hand, the maximum efficiency occurs for a DC voltage of 22V and a load level of 20%, the

worst efficiency occurs for a DC voltage of 30 V and a load level of 100% and the optimum operating point appears around 50% of the load.

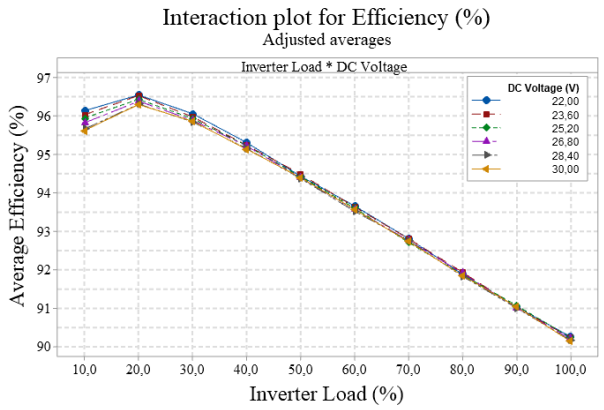

Fig. 14 Prototype II efficiency curves. Source: Own

TABLE X
ANOVA FOR THE EFFICIENCY OF THE PROTOTYPE II

Source	DF	SS	MS	Value F	Value P
Inverter Load (%)	9	520	57.78	9146.89	0.000
DC Voltage (V)	5	0.387	0.0773	12.24	0.000
Inverter Load (%) * DC Voltage (V)	45	0.329	0.0073	1.16	0.296
Error	60	0.379	0.0063		
Total	119	521.16			

Statistical Terms: DF = Degrees of Freedom; SS = Sum of Squares; MS = Mean Square.

Table X shows the ANOVA for the prototype II conversion efficiency

Observing the P values of each of the factors individually and their interaction, it can be ensured that the efficiency of the prototype II is dependent on the percentage of load and the variation of the DC voltage applied to the input, but it is independent of their interaction, as shown in Fig. 14.

Fig. 15, shows the graphic of normal probability for the efficiency of prototype II. Likewise, for a significance level of 0.05, it can be stated that the data follow the normal distribution line and that its behavior is as expected.

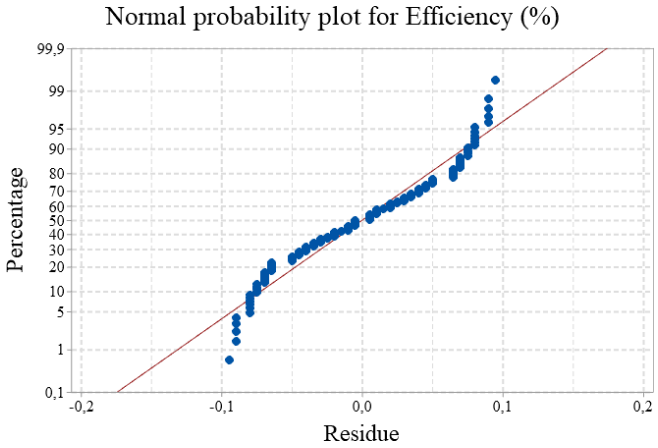

Fig. 15. Normal probability plot for the efficiency of the prototype II. Source: Own.

Tabla XI, presents the data of the THD produced by the prototype II. This second prototype has an average THD of 0.019% and according to the standard deviation, the data is less dispersed than in prototype I. Note that the amount of harmonics generated by prototype II is relatively less than that of prototype I, this is due to the location of the LC filter.

Fig. 16, presents the main effects plot for the prototype II THD. The behavior of the THD against load variations is different than in the prototype I, first, because its levels are below 0.035% and second, because between 30% and 90%, it is unstable. This unstable behavior is due to the resonance effect of the LC filter, which depends on the connected load [14] [15]. Note that there is an inversely proportional relationship between DC voltage and THD, for the same reason as in prototype I.

TABLA XII
ANOVA PARA LA EFICIENCIA DEL PROTOTIPO II

Fuente	DF	SS	MS	Valor F	Valor P
Inverter Load (%)	9	0.007	0.0008	1830.56	0.000
DC Voltage (V)	5	0.025	0.005	11346.6	0.000
Inverter Load (%) * DC Voltage (V)	45	0.013	0.0003	658.1	0.000
Error	60	0.0003	0.0063		
Total	119	0.045			

Statistical Terms: DF= Degrees of Freedom; SS = Sum of Squares; MS = Mean Square.

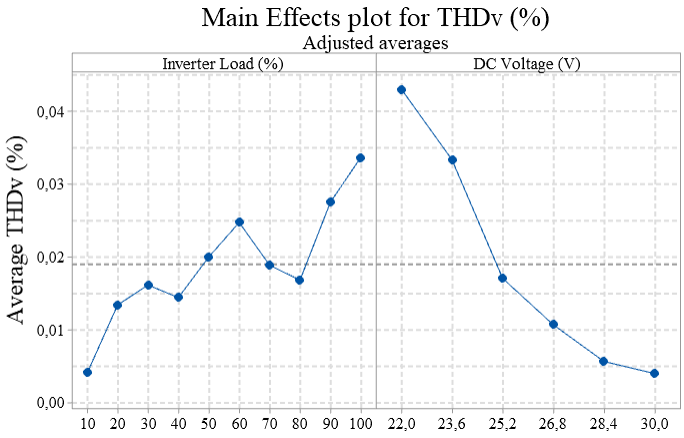

Fig. 16. Main Effects Plot for Prototype II THD. Source: Own.

Fig. 17, shows the interaction graph between the factors, where it can be clearly seen that both have an influence on the THD response.

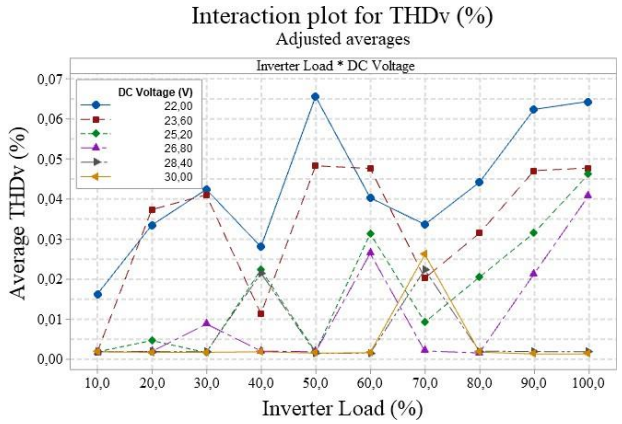

Fig. 17. THD curves of the prototype II. Source: Own

Similarly, it is observed that the THD presents an unstable behavior, for load values between 30% and 90% of the nominal, product of the resonant frequency of the LC filter. Note that for a DC voltage of 30 V, lower THD values are obtained, while for a voltage of 22 V, higher values are obtained. As future work, it is proposed to find a solution to the instability of these systems.

Table XII, shows the ANOVA for the THD of prototype II. Observing the P values of each of the factors and their interaction, it can be ensured that the THD of the prototype II is dependent on both the load percentage and the DC voltage, and also depends on their interaction, such as was shown in Fig. 17.

Fig. 18, shows the behavior of the collected data against the normal distribution line. This graph shows how the data tries to follow normality, but there is an oscillation, due to the instability of the response.

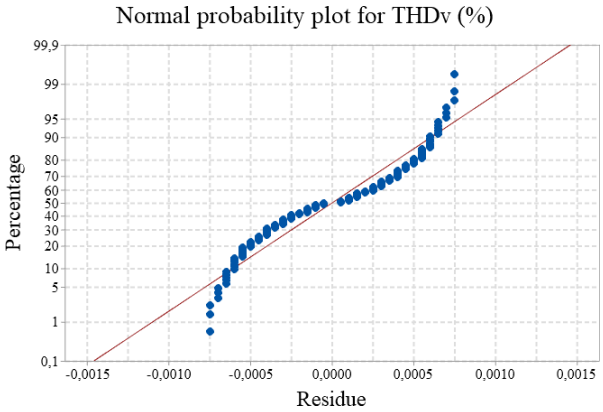

Fig. 18. Normal probability plot for the prototype II THD. Source: Own

Next, the hypotheses raised in Section II are validated for this particular prototype.

The hypothesis $H0_1$, It considers that the conversion efficiency and the THD are independent of the variation of the DC voltage, however, the results show that both the efficiency and the THD are dependent on the DC voltage. Therefore, the null hypothesis $H0_1$ is rejected and the alternate HA_1 is accepted.

The hypothesis $H0_2$, establishes that conversion efficiency , such as the THD, are independent of load percentage, nevertheless, the results show that both efficiency and THD, are dependent of load percentage, for that reason, the null hypothesis $H0_2$ is rejected and the alternate hypothesis HA_2 is accepted.

The hypothesis $H0_3$, affirms that conversion efficiency and the THD,are independent of interaction between DC voltage and load percentage, however, the results allow to affirm, that efficiency is independent of their interaction, but the THD is dependent. In this sense, both the null hypothesis $H0_3$, and the alternate hypothesis HA_3 are rejected.

The results obtained in this study align with and expand upon recent findings in the literature related to inverter performance in photovoltaic applications. For instance, the observation that the THD is significantly affected by both DC input voltage and output load is consistent with the analysis reported by Bouzguenda and Selmi [4], who emphasized the sensitivity of harmonic content to inverter design parameters and load conditions. Similarly, the higher efficiency observed when the LC filter is placed at the transformer's primary supports the conclusions of Shrestha et al. [3], who showed that minimizing transformer-conducted harmonics is key to reducing losses in transformer-based topologies.

Compared to the work of Albakri et al. [1], who provide a comprehensive overview of inverter designs, this study adds experimental insight by using a factorial design to quantify how controllable factors affect efficiency and harmonic distortion. Additionally, the THD levels achieved in both prototypes (under 1%) are in line with international standards such as IEEE 519 and EN 50160, validating the models under linear and resistive load assumptions —as also noted by Chaurasia and Singh [5] in their work on multilevel inverters.

Moreover, the instability observed in the THD under certain load conditions in prototype II may be associated with the resonant behavior of LC filters, as discussed in previous studies [2]. In particular, Horikoshi [13] examined how harmonic components originate and propagate in grid-connected photovoltaic inverters, emphasizing that both the selection and positioning of filter elements significantly influence waveform quality. This underscores the practical importance of not only choosing appropriate filter components but also strategically placing them within the circuit. The experimental methodology applied in this study, grounded in statistical rigor through ANOVA and controlled manipulation of input variables, offers a structured and replicable approach that is rarely found in similar simulation-based analyses, thereby enhancing the study's value in terms of reliability and applicability..

V. Conclusions

It was found that prototype I, the conversion efficiency is dependent on the load variation and independent of the variation of the DC voltage and its interaction, as an effect of placing the LC filter in the primary of the transformer. It was also observed that the THD is inversely proportional to the DC voltage and directly proportional to the load percentage.

It was observed that in the prototype II, the conversion efficiency is affected by the variations of the DC voltage and the percentage of connected load, but it is independent of the interaction of these two factors. On the other hand, the THD, despite being dependent on the DC voltage and the connected load, presents an unstable behavior for loads between 30% and 90% of the nominal power, due to the resonant effect of the LC network.

It was found that by placing the LC filter on the secondary of the transformer, the average efficiency of the converter is reduced because the high frequency harmonics are not attenuated and cause additional losses in the transformer, while the THD levels are slightly reduced.

It was observed that the THD levels obtained with the experiment, are much less than 1%, since during the experiment, it just consider linear loads and purely resistive, however, the analysis carried out provides an idea of how they are going to behave prototypes in front of non-linear loads and how they will affect the variation of the DC voltage and in the percentage of the connected load.

The resonant effect of LC network, generates instability on the response of the THD when it locates on the secondary of transformer, This highlights the need to minimize this effect in order to prevent high-power nonlinear loads from significantly degrading inverter performance and waveform quality.

It was found that by placing the LC filter on the secondary of the transformer, the average efficiency of the converter is reduced because the high frequency harmonics are not attenuated and cause additional losses in the transformer, while the THD levels are slightly reduced. This behavior is consistent with the findings of Gerardo and Miguel [16], who demonstrated that filter location significantly impacts both the harmonic suppression and energy losses in transformer-based inverter configurations

VI. Future Work and Contributions

The findings of this study provide a solid foundation for future developments in the design and optimization of DC/AC converters for off-grid photovoltaic systems. First, the experimental methodology used —based on factorial design and statistical validation— can be replicated to evaluate other converter topologies, modulation strategies (such as bipolar SPWM, space vector PWM), or filtering techniques. Additionally, the results highlight the importance of LC filter positioning in harmonic mitigation and system efficiency, offering practical guidance for designers seeking to optimize inverter layouts.

In future work, the prototypes could be tested under nonlinear and dynamic loads to simulate more realistic operating conditions. Also, implementing physical prototypes in laboratory settings will allow validation of the simulation results and the quantification of real-world losses, including thermal behavior and electromagnetic interference. Finally, this study opens the door to developing intelligent control systems that automatically adjust operating parameters (e.g., switching frequency, modulation index) based on load conditions, improving energy quality and system reliability in real-time.

By integrating these advances, the study contributes to the continuous improvement of photovoltaic systems, enabling more robust, efficient, and reliable off-grid energy solutions, particularly relevant for rural or remote electrification projects.

References

[1] M. Albakri, A. Darwish, and P. Twigg, “A Comprehensive Review of DC/AC Single-Phase Differential-Mode Inverters for Low-Power Applications,” *Electronics*, vol. 13, no. 13, p. 2474, 2024. https://doi.org/10.3390/electronics13132474.

[2] MDPI Energies, “A Comparative Review of Three Different Power Inverters for DC–AC Applications,” *Energies*, vol. 16, no. 21, p. 7254, 2023. https://doi.org/10.3390/en16217254

[3] S. Shrestha et al., “A Comparative Analysis of Transformer-less Inverter Topologies for Grid-Connected PV Systems,” *arXiv preprint arXiv:2501.08103*, 2025.

[4] M. Bouzguenda and T. Selmi, “Review of DC-AC converters for photovoltaic conversion chains,” *International Journal of Power Electronics and Drive Systems (IJPEDS)*, vol. 12, no. 2, pp. 886–901, 2021.https://doi.org/10.1007/978-981-19-7728-2_15

[5] R. Chaurasia and S. B. Singh, "Performance Analysis of Multi-level DC-AC Inverter for Solar Power Application," in *Recent Advances in Power Electronics and Drives*, Springer, 2023.https://doi.org/10.1007/978-981-19-7728-2_15 .

[6] H. Gutierrez and R. De la Vara, *Analysis and Design of Experiments*, 2nd ed., McGraw-Hill, 2016.

[7] G. A. Rampinelli, A. Krenzinger, and F. Chenlo Romero, “Mathematical models for efficiency of inverters used in grid connected photovoltaic systems,” *Renewable and Sustainable Energy Reviews*, vol. 34, pp. 578–587, 2014. https://doi.org/10.1016/j.rser.2014.03.047

[8] J. D. Gallego-Gomez, J. B. Cano-Quintero, and N. Muñoz-Galeano, “Deducción de pérdidas de potencia por conducción en inversores modulación senoidal de ancho de pulso, SPWM,” *Información Tecnológica*, vol. 26, no. 3, pp. 111–122, 2015. https://doi.org/10.4067/S0718-07642015000300015

[9] Busso, C. Cadena, and L. Vera, “Determinación de la eficiencia de conversión del inversor empleado en un sistema de generación fotovoltaica conectado a red instalado en el nordeste argentino,” *Avances en Energías Renovables y Medio Ambiente*, vol. 15, pp. 17–24, 2011.

[10] Beltrán Telles et al., “Análisis de calidad de la energía de inversor de puentes H y control SPWM,” *Ingeniería Energética*, vol. 41, no. 1, pp. 1–11, 2020.

[11] D. Montgomery, *Design and Analysis of Experiments*, 8th ed., Wiley, 2012.

[12] E. Lázaro Campo, *Optimización del índice de producción final de una instalación solar fotovoltaica para un inversor y emplazamientos dados*, Tesis de Maestría, 2012.

[13] Horikoshi, *Análisis de las componentes armónicas de los inversores fotovoltaicos de conexión a red*, Tesis de Maestría, 2009.

[14] R. A. da Câmara et al., “Comparative analysis of performance for single-phase AC-DC converters using FPGA for UPS applications,” in *Proc. IEEE APEC*, 2013, pp. 1852–1858. https://doi.org/10.1109/APEC.2013.6520547

[15] R. Federico Farfán and C. Wilhelm Massen, “Análisis de dos modelos matemáticos de inversores para el estudio de la variación de la eficiencia de conversión con respecto a la tensión de entrada,” 2018. https://doi.org/10.59627/cbens.2018.281

[16] V. Gerardo and S. J. Miguel, “High Efficiency Single-Phase Transformer-less Inverter for Photovoltaic Applications,” *Ingeniería Investigación y Tecnología*, vol. XVI, no. 2, pp. 173–184, 2015. https://doi.org/10.1016/j.riit.2015.03.002

Johan Fernández Zorro. Sogamoso native, Colombia. Received a degree in Electronic Engineering from Universidad Pedagógica y Tecnológica de Colombia, located in Sogamoso, Colombia 2020. He is teacher from Electronic Engineering School from Universidad Pedagógica y Tecnológica de Colombia. He works in Future Solutions Development S.A.S Company as research engineer.
https://orcid.org/0000-0003-2905-5438

Nairo Julian Rodriguez Ballesteros is an junior researcher at the Sena centro industrial de mantenimiento y manufactura. He works as leader in research group, innovation and applied knowledge of boyaca (GICAB- SENA) in reliability engineering. He received his B.Sc. in electromechanical engineering from Universidad pedagógica y tecnológica de Colombia in 2009 and holds a M.Sc. in engineering- mechanical from the Universidad Nacional de Colombia, (2015). https://orcid.org/0000-0001-8471-1579

Elkin Wbeimar Suarez Chaparro Sogamoso native, Colombia. Received a degree in Electronic Engineering from Universidad Pedagógica y Tecnológica de Colombia, located in Sogamoso, Colombia Colombia 2017. he is and hardware developer , and amateur embedded programmer , works in Power electronics, oriented to photovoltaic energy appliances, actually he works like senior research at Future Solutions Development S.A.S company.
https://orcid.org/0000-0002-2721-5605

Model of an ideal Rankine cycle with reheating in E.E.S.

Modelamiento de un ciclo Rankine ideal con recalentamiento en E.E.S.

D. A. Narváez-Meza.

DOI: https://doi.org/10.22517/23447214.25773
Scientific and technological research paper

***Abstract*— In the present study, a comprehensive analysis is carried out on an ideal regenerative Rankine cycle, based on the use of ICT tools for digital transformation in engineering education. The gap addressed in this work relates to the application of technologies to streamline the thermodynamic analysis of complex cycles, which have been rigorously modeled using the Engineering Equation Solver (E.E.S.) software a high-fidelity computational tool widely recognized for its accuracy in solving nonlinear, multivariable thermodynamic systems. The methodological approach adopted involves a detailed evaluation of the isentropic efficiencies of the main cycle components turbines, pump, and heat exchangers enabling a precise determination of the net power output, the rates of thermal energy transfer to and from the heat exchangers, as well as the quantification of the mass flow rates of extracted steam at specific points in the system for regenerative purposes. Additionally, the computational generation of temperature–entropy (T–s) diagrams is integrated, which serve as fundamental tools for the visualization and validation of the thermodynamic processes involved, allowing for the clear identification of each state in the cycle. Based on this graphical representation and the numerical results derived from the model, key thermodynamic properties are determined, such as specific volume at pump suction, entropy at turbine inlet, and enthalpies associated with each energy transformation, in order to quantitatively establish the isentropic efficiency of the devices and their influence on the overall efficiency of the regenerative cycle. This approach enables not only a comprehensive understanding of system behavior but also the identification of improvement opportunities for the energy optimization of advanced thermoelectric cycles.**

***Index Terms*— Efficiency; isentropic; Rankine cycle; regeneration; reheating; turbine.**

Este artículo de investigación fue sometido a revisión el 04 de Febrero de 2025, aceptado el 12 de Junio de 2025 y publicado el 30 de Junio de 2025. Fue financiado en el marco del proyecto CIP de sistemas avanzados aplicados a modelos termodinámicos de la Corporación Universitaria Autónoma de Nariño, la Universidad Mariana de Colombia y el grupo de investigación CEDMATEC. El estudio se llevó a cabo como un capítulo preliminar del libro doctoral sobre energía eólica del candidato a doctorado Favio Nicolás Rosero y tiene como objetivo analizar las fuentes de energía que pueden aplicarse en el departamento de Nariño, explorando la capacidad de energía eólica y geotérmica del departamento, con base en el estudio energético del profesor Diego Alejandro Narváez (dienarvaez125@umariana.edu.co, diego.narvaez@aunar.edu.co)

***Resumen*— En el presente estudio se desarrolla un análisis exhaustivo de un ciclo Rankine regenerativo ideal basado en el uso de herramientas TIC para la transformación digital en la enseñanza de la ingeniería, la brecha que se pretende abordar se enmarca en el uso de las tecnologías para agilizar los análisis termodinámicos de ciclos complejos, los cuales han sido rigurosamente modelado mediante el uso del software Engineering Equation Solver (E.E.S.), una herramienta computacional de alta fidelidad ampliamente reconocida por su precisión en la resolución de sistemas termodinámicos no lineales y multivariable. El enfoque metodológico adoptado contempla la evaluación minuciosa de las eficiencias isoentrópicas de los principales componentes del ciclo, turbinas, bomba e intercambiadores de calor, lo cual permite una determinación precisa de la potencia neta generada, las tasas de transferencia de energía térmica hacia y desde los intercambiadores, así como la cuantificación de los flujos másicos de vapor extraído en puntos específicos del sistema para efectos regenerativos. Asimismo, se integra la generación computacional de diagramas temperatura –entropía (T–s), los cuales constituyen herramientas fundamentales para la visualización y validación de los procesos termodinámicos involucrados, permitiendo la identificación clara de cada uno de los estados del ciclo. A partir de esta representación gráfica y de los resultados numéricos derivados del modelo, se determinan propiedades termodinámicas clave.**

***Índice de términos*— Ciclo de Rankine; eficiencia; isentrópico; recalentamiento; regeneración; turbina.**

I. INTRODUCCIÓN

El ciclo Rankine ideal con recalentamiento y regeneración, es un proceso utilizado en centrales eléctricas de vapor que se logra por la extracción del vapor o también denominado drenaje del mismo de la turbina de alta presión, el vapor extraído en la región de vapor sobrecalentado que en el ciclo Rankine ideal simple no produce trabajo, se pasa nuevamente por la caldera para elevar su temperatura bajo la misma línea de presión de extracción, incrementando la entropía del vapor realizando una expansión isoentrópica hasta la salida de la turbina de baja presión.

Es importante recalcar que existen algunas recomendaciones para incrementar la eficiencia isoentrópica además de algunas limitaciones en el estudio de variables termodinámicas que se pueden abordar aplicando herramientas de transformación digital.

La propuesta del presenta artículo se basa en el objetivo general el cual pretende aplicar las herramientas TIC del curso CIP de sistemas avanzados aplicados a modelos termodinámicos basados en el software EES como lo propone Fernández, *et al* (2020) en su investigación sobre TIC aplicadas en la enseñanza de la ingeniería mecánica [1], como herramienta computacional para el análisis de diferentes ciclos termodinámicos como los ciclos de vapor, ciclos de refrigeración y la posibilidad de la exploración de energía geotérmica en el volcán Cumbal en fuentes hiper entálpicas, además del análisis de ciclos de refrigeración en general.

II. METODOLOGÍA APLICADA

Desde una perspectiva metodológica de tipo exploratoria, este estudio parte de la necesidad de indagar cómo la implementación del software *Engineering Equation Solver* (E.E.S.) puede facilitar la comprensión y resolución de ciclos de vapor Rankine con recalentamiento en el contexto de la formación en ingeniería generando en los estudiantes competencias tecnológicas dentro de la mecánica aplicada, en el análisis termodinámico aplicado a la docencia, se plantea como hipótesis exploratoria que el uso del E.E.S como se evidencia en los estudios de Medina et al. (2024) el cual permite un análisis detallado y una comprensión más profunda de los temas tratados acorde a la literatura actual, la interpretación teórica, el enfoque pedagógico y un análisis de elementos previos de hipótesis planteada [2], permite no solo modelar con mayor precisión los procesos involucrados en un ciclo Rankine con recalentamiento, sino también fomentar en los estudiantes una comprensión más profunda de las relaciones entre eficiencia, condiciones de operación y transformaciones energéticas clave.

III. MARCO TEÓRICO.

A) Aprendizaje basado en herramientas tecnológicas

Acorde a los estudios previos sobre herramientas tecnológicas aplicadas a la educación, se propone una estrategia que le permita al estudiante desarrollar habilidades tecnológicas dentro de la mecánica computacional, propendiendo por la calidad en el ejercicio docente, estas herramientas tecnológicas permiten la reducción de brechas generando en el docente didácticas en el aula que permitan una apropiación del conocimiento mediado por las TIC, es asi que Mosquera (2021) en su estudio denominado "Factores asociados al uso de tecnologías de la información y la comunicación (TIC) en los procesos de aprendizaje de estudiantes de ingeniería", en el cual se evidencia la importancia del uso de las TIC en estudiantes universitarios cuyas experiencias son significativas mejorando el perfil del egresado, mejorando las competencias digitales transversales bajo los constructos del modelo propuesto [3]. Por este motivo es importante entender que el uso de herramientas tecnológicas además de desarrollar habilidades digitales, reduce las brechas educativas en el contexto regional, el aprendizaje mediado por soluciones tecnológicas especializadas contribuye a los procesos de cualificación profesional, pues esta se orienta a mejorar las dinámicas sociales y educativas del entorno.

B). Métodos de Reducción de presión en el sumidero:

El fluido de trabajo existe dentro del sumidero como un vapor húmedo a la temperatura de saturación de la salida de la turbina de baja presión, la reducción de la presión de operación del condensador disminuye la temperatura del vapor, la reducción de la presión incrementa la eficiencia del ciclo Rankine como se puede observar en la figura. Según Hernández, Zumalacárregui & Pérez (2020) permite disminuir en mayor medida la presión de trabajo en el condensador lo que permite incrementar la eficiencia térmica del ciclo Rankine, tal como se puede apreciar en la Fig. 1. Del diagrama T vs s del ciclo [4].

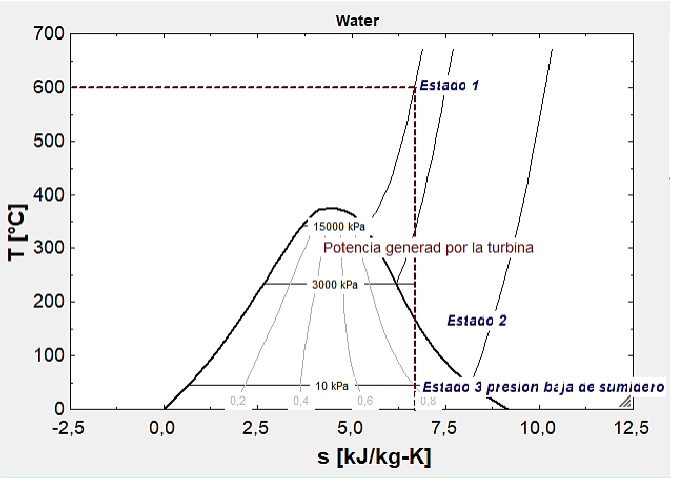

Fig. 1. Reducción de presión del sumidero, fuente: Esta investigación, parametrización en E.E.S.

El proceso de expansión de un gas, representa un proceso adiabático reversible también denominado isoentrópico, para los parámetros establecidos la entropía del sistema es de $6{,}67\frac{kJ.k}{kg}$, de acuerdo a los parámetros establecidos en el software E.E.S como se observa en los resultados de la Fig. 2.

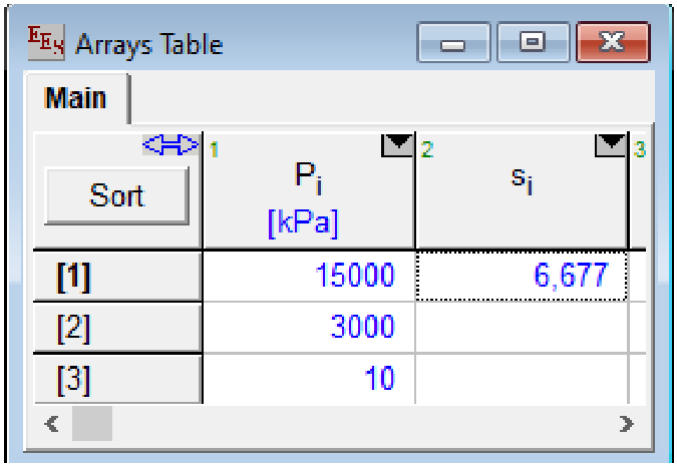

Fig. 2. Entropía específica calculada mediante EES pasados en las presiones 15000 kPa, 3000 kPa y 10 kPa. Fuente: Esta investigación, parametrización en E.E.S.

Basados en los procesos de entropía constante se realiza el análisis isoentrópico de la turbina teniendo en cuenta que el cálculo se realiza desde el punto de vista ideal, donde no se tiene en cuenta las irreversibilidades de un proceso.

C). Recalentamiento del vapor de extracción:

Después de la extracción de vapor de la turbina de alta presión pasa nuevamente por la caldera, incrementando la temperatura del fluido de trabajo, la presión se mantiene constante desde la extracción del vapor sobrecalentado, hasta el ingreso a la turbina de baja presión, el vapor se calienta nuevamente generando expansión en la misma incrementando la potencia producida por la turbina, como se muestra en la siguiente ecuación de balance de energías y su desarrollo. De acuerdo a lo planteado por Vásquez & Carbajal (2020) se evidencia resultados satisfactorios con respecto a la influencia en el incremento de temperatura a las entradas de la turbina, es por esta razón que aplicando un recalentamiento se aprovecha la energía del fluido para incrementar la salida de potencia neta de la turbina e incrementar la eficiencia térmica del ciclo [5]. El balance de energías de primera ley tal como se puede apreciar en (1) acorde al texto Çengel & Boles (2021) donde se evidencia las variaciones de energía de un sistema [6].

$$Ein - Eout = \Delta E\ sistema \quad (1)$$

Donde:

1. $Ein = Energía\ de\ entrada$

2. $Eout = Energía\ de\ salida$

3. $\Delta E\ sistema = Cambios\ de\ energía\ del\ sistema$

Los cambios de energía del sistema se presentan cuando el régimen estudiado es transitorio; sin embargo, dentro de las consideraciones las propiedades tanto a la entrada como a la salida se mantienen constantes, de esta manera se determina el régimen estacionario de los equipos, las energías presentes se reemplazan en (1) acorde a las formas de entrada y salida de las mismas y las variaciones del sistema.

$$(Qin + Win + Ein) - (Qout + Wout + Eout) = \Delta E\ sistema$$

Donde:

1. $Qin = Calor\ de\ entrada$
2. $Qout = Calor\ de\ salida$
3. $Win = Trabajo\ de\ entrada$
4. $Wout = Trabajo\ de\ salida$

Reemplazando el análisis de primera ley (1) para cada uno de los estados

$$\dot{m}.(h1 - h2) + \dot{m}.(h3 - h4) = \dot{W}neto$$

Donde

1. $\dot{m} = Flujo\ másico\ [\frac{kg}{s}]$

2. $h1, h2, h3\ y\ h4 = Entalpia\ especifica\ [\frac{kJ}{kg}]$

Con el recalentamiento se incrementa la eficiencia neta de la turbina, el vapor recalentado se utiliza para producir potencia en la segunda etapa de la turbina de alta presión como se muestra en la figura 4, de esta manera se aumenta la potencia total de la turbina sumando la primera etapa de alta presión y la segunda etapa de baja presión aprovechando la alta entalpia de la extracción y pasando este vapor nuevamente por la caldera. El análisis del Ciclo Rankine con recalentamiento en el programa EES (Engineering Equation Solver) representa una herramienta fundamental en la enseñanza de la Termodinámica, ya que permite a los estudiantes modelar sistemas térmicos reales con mayor precisión y comprender el impacto de los diferentes componentes del ciclo sobre su eficiencia.

Este tipo de ciclo, utilizado comúnmente en centrales termoeléctricas, incorpora una etapa adicional de calentamiento del vapor después de su expansión parcial, lo que contribuye a mejorar la eficiencia térmica del sistema y a reducir la humedad al final de la expansión en la turbina. Mediante el uso de EES, los estudiantes pueden visualizar los cambios de estado del fluido de trabajo en los diagramas T-s y h-s, calcular propiedades termodinámicas con gran exactitud y realizar balances de energía en cada componente.

Además, el entorno de programación de EES fomenta el pensamiento crítico y el análisis comparativo, ya que permite modificar parámetros como presiones, temperaturas y niveles de recalentamiento para observar su efecto directo sobre la eficiencia del ciclo.

Esta experiencia práctica no solo fortalece el aprendizaje conceptual de la Termodinámica, sino que también prepara a los futuros ingenieros para enfrentar desafíos reales en el diseño y optimización de sistemas energéticos. Los valores de la presión de sumidero corresponden a 10 kPa a la salida de la turbina en su segunda etapa de recalentamiento como se puede evidenciar en la Fig. 3.

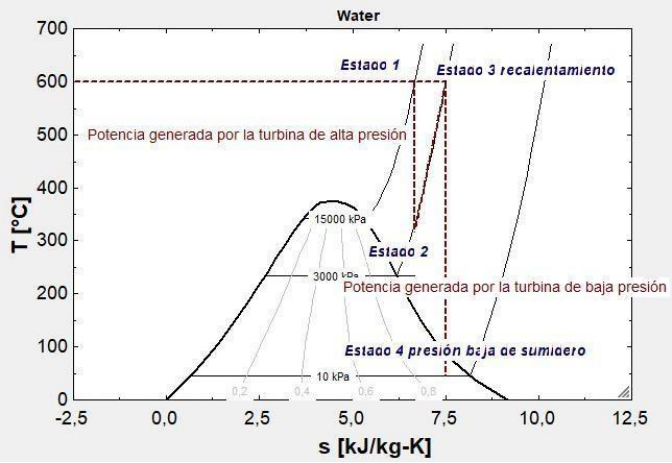

Fig. 3. Recalentamiento de los estados 3 y 4, Fuente: Yunes A. Cengel Termodinámica, capítulo 10. Efecto que produce incrementar la presión de la caldera en el ciclo Rankine ideal y bajar la presión de sumidero línea roja punteada. Fuente: El autor, ciclo programado en E.E.S.

D) Expansión isoentrópica de la turbina de alta presión.

Mediante la presión de la turbina de alta al ingreso del fluido de trabajo, se determina la entropía y entalpia del estado 1 antes de la expansión del vapor, al ser un análisis ideal de la turbina de alta presión se supone que el elemento es diabático reversible por lo tanto corresponde a un proceso isoentrópico. Donde la entropía específica al ingreso y después de la expansión del gas es igual en un proceso adiabático reversible tal como se muestra en la Fig. 4 para los estados 1 y 2.

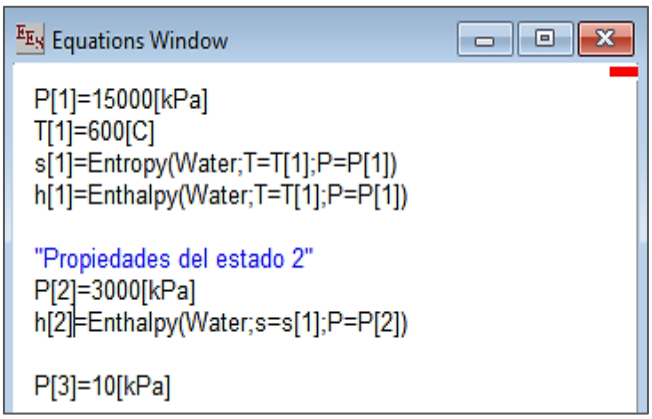

Fig. 4. Programación en EES de las propiedades termo físicas para los estados 1 y 2. Fuente: Esta investigación, software E.E.S.

Con los valores de la entropía específica del estado 2 y la presión de 3000 kPa encontramos la entalpia específica y la temperatura a la salida de la turbina de alta presión en los estados 1 y 2 tal como se observa en la Fig. 5.

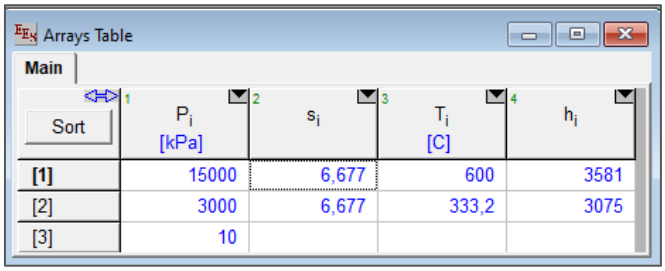

Fig. 5. Tabla de valores termodinámicos de los estados 1 y 2. Fuente: Esta investigación, software E.E.S.

Basados en la tabla generada por el E.E.S. definimos las curvas paramétricas en el eje x como entropía específica y en el eje y temperatura, como se muestra en la figura 6.

E) Diagrama T-s expansión isoentrópica de la turbina de alta presión

Como es de esperarse las entropías a la entrada y salida de la turbina son iguales, con estas propiedades en el software E.E.S. se puede determinar las temperaturas de salida de la turbina y la entalpia específica, como se puede observar en la Fig. 6.

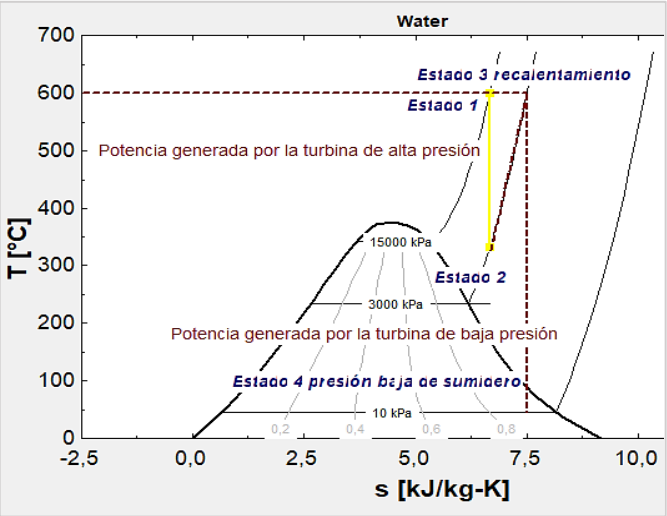

Fig. 6. Parametrización propiedades termo-físicas en E.E.S. para los ejes x, y respectivamente sobre el diagrama T-s. Fuente: Esta investigación, software E.E.S.

F) Expansión isoentrópica de la turbina de baja presión

Las propiedades termodinámicas se parametrizan bajo el código de programación en EES, se determina presión, entropía específica y temperatura como se aprecia en la Fig. 7. Este paso es necesario ya que se van a trabajar valores de temperatura entropía, caso contrario se debe parametrizar los valores de temperatura en cada uno de los estados o cambiar el modelo gráfico con las propiedades existentes en tabla.

Arrays Table

Main

Sort	P_i [kPa]	s_i [kJ/kg-K]	T_i [C]	h_i [kJ/kg]
[1]	15000	6,677	600	3581
[2]	3000	6,677	333,2	3075
[3]	3000	7,508	600	3682
[4]	10	7,508	45,82	2380

Fig. 7. Propiedades termodinámicas de los estados 1 al 4 del ciclo Rankine con recalentamiento. Fuente: Esta investigación

G) Eficiencia del ciclo Rankine ideal con recalentamiento

Uno de los principales objetivos del recalentamiento con respecto al incremento de la eficiencia térmica de los ciclos de vapor, está basada en aprovechar la mayor cantidad de potencia suministrada por la turbina, reducir la presión del sumidero y volver el ciclo eficiente a diferencia del ciclo Rankine simple. Ortega (2024) afirma que adicionalmente el trabajar con fluidos orgánicos incluyen la eficiencia de recuperación de calor de los desechos térmicos además de la reducción de las emisiones de gases de efecto invernadero [7]. Por lo tanto, aportan significativamente a la sostenibilidad ambiental, a diferencia de los ciclos convencionales. A continuación, se evidencia el cálculo de la eficiencia térmica del ciclo Rankine ideal con recalentamiento y el diagrama T-s para los 6 estados correspondientes Fig. 6. Es así que Smith y Brown (2020) en su investigación infieren en los diferentes métodos de recalentamiento y como afecta la eficiencia térmica de un ciclo termodinámico [8].

IV. ANALISIS DE RESULTADOS

De acuerdo a los resultados obtenidos para los 6 procesos termodinámicos y el recalentamiento que se propone para mejorar la eficiencia térmica, se evidencian los siguientes aspectos respecto a cada uno de los estados.

Estado 1-2: Expansión isoentrópica Del vapor sobrecalentado.

Estado 2-3: Recalentamiento del vapor a presión constante (Isobárico)

Estado 3-4: Expansión isoentrópica del vapor sobrecalentado a zona de mezcla.

Estado 4-5: Saturación de la mezcla a estado líquido.

Estado 5-6: Incremento de la presión, paso por la bomba.

Estado 6-1: Adición de calor a presión constante, entrada de la caldera.

A) Descripción del Ciclo Rankine con Recalentamiento

El ciclo Rankine con recalentamiento de diferentes etapas que se describen de manera detallada, existe una expansión isoentrópica en la turbina de lata presión, además se realiza en la extracción un recalentamiento para aprovechar la entalpía existente, de esta manera el vapor en estado sobrecalentado se regresa a la caldera, con el objetivo de incrementar el potencial energético del fluido con el fin de producir trabajo en una segunda etapa como se puede observar en la figura 8.

El recalentamiento en un ciclo Rankine es un proceso termodinámico que consiste en aumentar la temperatura del vapor después de una primera expansión parcial en la turbina, con el fin de mejorar la eficiencia del ciclo y reducir la humedad del vapor en las etapas finales de expansión. En el contexto de un ciclo Rankine con recalentamiento, este proceso ocurre típicamente entre dos niveles de presión: alta presión y baja presión.

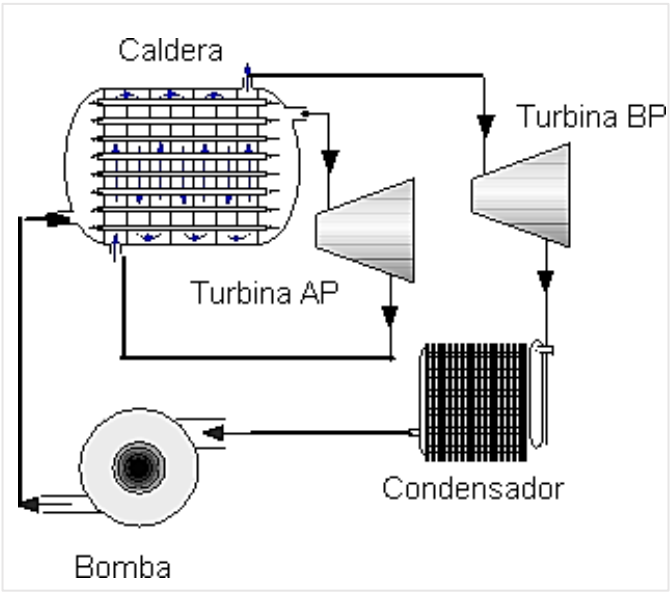

Fig. 8. Ciclo Rankine idea con recalentamiento, fuente: Esta investigación, diseño en EES.

1. **Bomba de alimentación de la turbina de alta presión:** El agua a alta presión es enviada a la caldera.

- Estado 5-6.

2. **Caldera:** El agua es convertida en vapor seco a alta presión, lleva el vapor a la región sobrecalentada en el domo.

- Estado 6 -1 primera etapa de calentamiento

- Estado 2-3 segunda etapa de calentamiento.

3. **Turbina de alta presión (TAP):** El vapor expandido entrega trabajo útil al eje de la turbina, es donde se produce la máxima potencia.

4. **Recalentador:** Después de la expansión inicial en la turbina de alta presión, el vapor es recalentado para aumentar su temperatura antes de ser enviado a la turbina de baja presión, con el fin de aprovechar la alta energía del vapor expandido dentro de la primera etapa.

5. **Turbina de baja presión (TBP):** El vapor recalentado se expande nuevamente, generando trabajo adicional.

6. **Condensador:** El vapor se condensa nuevamente en líquido, completando el ciclo para ser llevado a la bomba de alimentación.

Los estados mostrados se programan acorde a las variables termo físicas presentes en la Fig.9. con los valores de temperatura, presión, entropía del sistema.

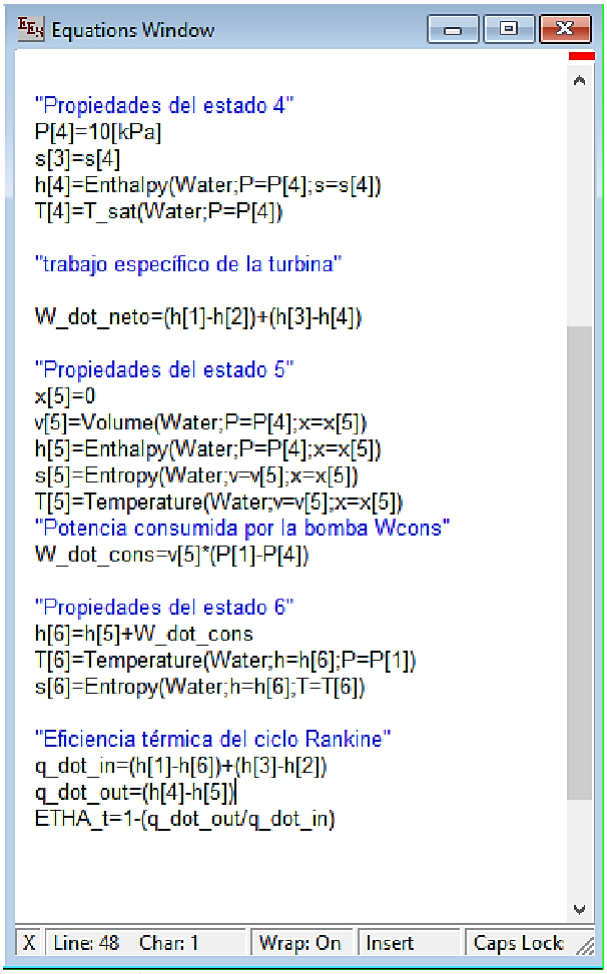

Fig. 9. programación del ciclo Rankine ideal con recalentamiento en EES fuente: esta investigación.

Para el análisis de un ciclo Rankine con recalentamiento se debe entender como una mejora del ciclo Rankine ideal simple, en el cual el vapor generado se expande parcialmente en una turbina, luego se vuelve a calentar a alta presión antes de continuar su expansión. Este proceso aumenta la eficiencia térmica del ciclo y reduce la humedad del vapor al final de la expansión.

Para la parametrización de un ciclo Rankine con recalentamiento, es fundamental comprenderlo como una evolución del ciclo Rankine ideal simple, diseñado específicamente para superar algunas de sus limitaciones térmicas y mecánicas. En este ciclo mejorado, el vapor inicialmente generado se expande en una turbina de alta presión hasta alcanzar una condición intermedia; luego, en lugar de continuar su expansión directamente, se redirige nuevamente a la caldera o generador de vapor, donde se somete a un proceso de recalentamiento a presión constante.

Este vapor recalentado, de mayor temperatura y energía, se introduce entonces en una segunda turbina de baja presión para completar su expansión hasta el condensador, de esta manera se aprovecha la potencia neta de la turbina en una segunda etapa, como se puede observar en la Fig. 10. Para el recalentamiento entre los estados 3 y 4 en la expansión isoentrópica del sistema.

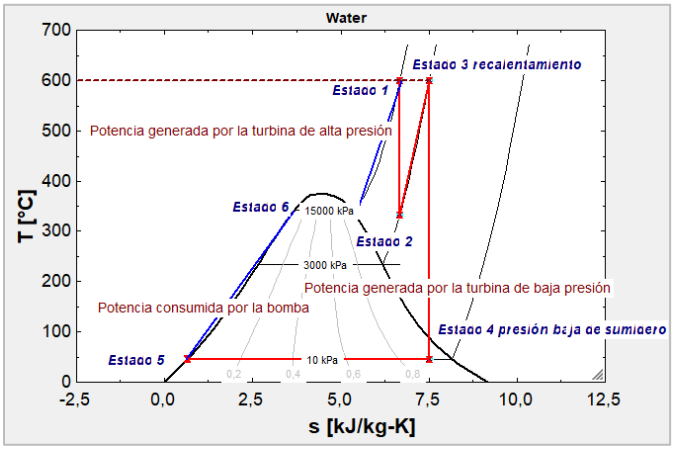

Fig. 10. Estados termodinámicos del ciclo Rankine ideal con recalentamiento, fuente: Esta investigación.

Se determina la eficiencia térmica con los valores del calor de salida del sumidero y el calor de entrada al ciclo de recalentamiento.

B) Potencia de una turbina

Para determinar la potencia de una turbina isoentrópica se toma las entalpías de entrada h1 y salida h2 aplicando la ecuación de la primera ley de la termodinámica para sistemas abiertos en estado estacionario, considerando el trabajo realizado por la turbina ver Fig.11. para el flujo de masa suministrado; sin embargo, se calculará la potencia por unidad de masa tomando las entalpias específicas de las tablas termodinámicas o los valores tomados del EES.

Se puede determinar que, al calcular la potencia de una turbina bajo condiciones isoentrópicas utilizando entalpías específicas obtenidas de tablas o del software E.E.S., se obtiene una estimación ideal del trabajo mecánico máximo aprovechable. Esta aproximación ignora las irreversibilidades internas propias del proceso real, como fricción y pérdidas térmicas; sin embargo, estas no fueron consideradas en el estudio.

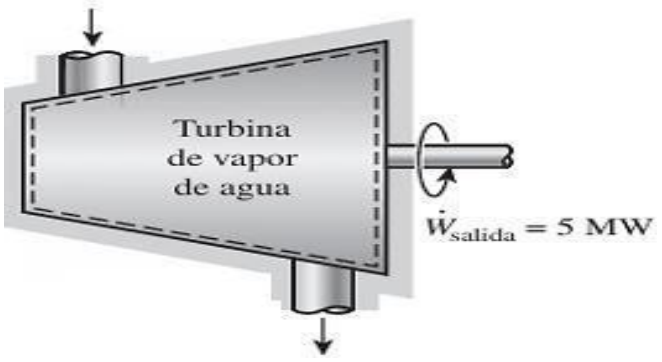

Fig. 11. Sistemas abiertos, turbina isoentrópica de 5 MW. Fuente: Cengel Termodinámica.

Análisis de primera ley para sistemas abiertos en estado estacionario, propiedades a la entrada de la turbina en una eexpansión isoentrópica del vapor sobrecalentado, tal como se puede apreciar en (2) acorde al texto Çengel & Boles (2021) correspondiente a un análisis de régimen estacionario en (2) [6].

$$\dot{E}_{in} - \dot{E}_{out} = \frac{\dot{\Delta E, sistema}}{dt} \qquad (2)$$

Donde:

- W es la potencia de la turbina por unidad de masa en kJ/kg.
- h1 es la entalpía específica de entrada (en kJ/kg).
- h2 es la entalpía específica de salida (en kJ/kg).

$$\dot{W}_{Turbina} = h1 - h2 \qquad (3)$$

$$\dot{W}_{Turbina} = 3581 \frac{kJ}{kg} - 3075 \frac{kJ}{kg}$$

$$\dot{W}_{Turbina} = 506 \frac{kJ}{kg}$$

La salida de la turbina de alta presión aun contiene una energía alta por lo tanto se genera un recalentamiento pasando nuevamente la línea de vapor para pasarlo por una turbina de baja presión. La potencia de la turbina en su primera etapa se determina mediante el análisis de primera ley para un régimen estacionario el cual se puede apreciar en (3) acorde al texto Çengel & Boles (2021) análisis de primera ley para un equipo adiabático reversible para los estados 1 y 2 [6].

C) Potencia de la turbina de baja presión:

I.

La modelación del ciclo Rankine ideal con recalentamiento según Sánchez (2016) tiene como beneficio según frente a otros programas convencionales la incorporación de las tablas de propiedades de trabajo, ahorrar mucho tiempo en la resolución de problemas frente al método tradicional, de interpolación manual de las entalpías específicas, se puede emplear en realizar análisis de sensibilidad y ayudar a una mejor comprensión del principio de funcionamiento de los sistemas termodinámicos, equipos y la variación de las propiedades de los fluidos [9]. Acorde al texto Çengel & Boles (2021) en (4) y (5) para determinar la potencia en la segunda etapa de la turbina y la potencia neta total del sistema [6].

$$W^{\cdot}_{Turbina} = h3 - h4 \quad (4)$$

$$W^{\cdot}_{Turbina} = 3682\ \frac{kJ}{kg} - 2380\ \frac{kJ}{kg}$$

$$W^{\cdot}_{Turbina/baja} = 882\ \frac{kJ}{kg}$$

Potencia neta:

$$W^{\cdot}_{neto-Turbina} = \sum W\ Turbina \quad (5)$$

$$W^{\cdot}_{neto-Turbina} = 506\ \frac{kJ}{kg} + 882\ \frac{kJ}{kg}$$

La eficiencia térmica de un ciclo Rankine con recalentamiento se determina cuantificando los calores de entrada y salida del sistema, estos valores tienden a ser bajos debido a las diferentes irreversibilidades; sin embargo, se puede determinar mediante (5) acorde al texto Çengel & Boles (2021) para determinar la eficiencia de los diferentes ciclos de vapor basados en el ciclo Rankine simple y Rankine con recalentamiento [6].

$$n(t\acute{E}rmica) = 1 - \frac{q_{out}}{q^{\cdot}_{in}} \quad (5)$$

$$n(t\acute{E}rmica) = 1 - \frac{h4 - h5}{(h1 - h6) + (h3 - h2)}$$

$$n(t\acute{E}rmica) = 1 - \frac{2188\ kJ/kg}{3982\ kJ/kg}$$

$$n(t\acute{E}rmica) = 45\%$$

Se aprecia la eficiencia térmica en el software EES un valor de 45,06%, como se puede apreciar en la tabla 1. De acuerdo a lo anterior Johnson y Williams (2019) en su investigación infieren que el recalentamiento mejora la eficiencia térmica de un ciclo Rankine, aumentando la potencia suministrada por la turbina mejorando el sistema operativo real de una planta [10]. De acuerdo a los parámetros establecidos la eficiencia térmica del ciclo termodinámico mejora considerablemente; sin embargo, es importante recalcar que dicho calculo corresponde a la eficiencia isoentrópica del ciclo termodinámico por lo que su eficiencia real puede disminuir en el análisis.

Acorde a las investigaciones realizadas por Zobeiry, N., & Humfeld, K. D. (2021). En el cual se expone de forma integral los desafíos inherentes a la modelación y control térmico en procesos de manufactura, particularmente cuando se involucran fenómenos complejos gobernados por Ecuaciones en Derivadas Parciales (EDPs), Como la conducción y convección de calor [11]. Tradicionalmente, tales problemas se abordan mediante métodos numéricos como los Elementos Finitos (FE), que, si bien son rigurosos y físicamente fundamentados, presentan limitaciones en cuanto a la rapidez computacional, lo cual presenta limitaciones que pueden ser resueltas mediante herramientas específicas de solución como evidencia en la Fig. 12.

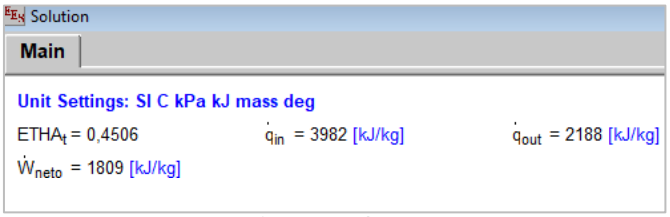

Fig. 12. Calculo de las eficiencias térmicas del ciclo Rankine con recalentamiento en EES. Fuente: Esta investigación EES.

La eficiencia térmica de un ciclo Rankine ideal no supera el 35% por lo que aplicar un recalentamiento puede incrementar la eficiencia hasta un 15%, llegando a un 45% con respecto al ciclo Rankine ideal simple provechando la potencia producida en la etapa de recalentamiento.

Acorde a los estudios realizados por Olivera Cosgalla & Sánches (2021) aluden que siempre es importante poder medir y comparar los resultados obtenidos contra patrones establecidos, por lo que los métodos de análisis experimentales, es importante contrastar los elementos de la mecánica computacional y los fenómenos de la vida real; sin embargo, son buenas aproximaciones al análisis termodinámico [12].

VI. CONCLUISONES

La simulación en EES del ciclo Rankine ideal con recalentamiento demostró un notable incremento en la eficiencia térmica del sistema, alcanzando un 45%. Este aumento significativo resalta la efectividad del recalentamiento como estrategia para mejorar el rendimiento de los ciclos de generación de energía.

Con respecto a la reducción de la presión del sumidero a 10 kPa contribuyó considerablemente a la mejora de la eficiencia del ciclo Rankine. La disminución de la presión del condensador permite un mayor aprovechamiento del trabajo útil en la turbina, optimizando así la conversión de energía térmica en energía mecánica. La implementación del recalentamiento en el ciclo Rankine no solo mejoró la eficiencia térmica, sino que también ayudó a reducir las tensiones térmicas en la turbina. Esto puede resultar en una mayor vida útil de los componentes y una operación más fiable del sistema de generación de energía.

Los valores tomados dentro de los rangos de presión de ingreso a la turbina, expansión isoentrópica y una segunda expansión para el recalentamiento, representa un incremento significativo en la eficiencia térmica de un ciclo, es importante tener en cuenta que el incremento de la potencia producida depende de factores como la diferencia de presión entre el sumidero y la salida en la segunda etapa.

Los resultados obtenidos del presente estudio modelado mediante el software *Engineering Equation Solver* (E.E.S.), permiten concluir que esta herramienta tecnológica representa un recurso valioso en la enseñanza y comprensión de sistemas termodinámicos complejos en ingeniería mediados por el uso de las TIC. Si bien el enfoque exploratorio de este estudio no permite una validación estadística formal, la experiencia de modelado y visualización de los procesos involucrados sugiere que el uso de E.E.S. favorece la comprensión de las variables termo físicas que influyen en la eficiencia del ciclo, así como una mayor claridad en la identificación de transformaciones energéticas críticas.

VII. RECOMENDACIONES

Dentro del estudio es importante tener en cuenta que el software es una aproximación matemática significativa, sin embargo para el caso no se tienen en cuenta las eficiencias de los equipos por lo que el rendimiento real del ciclo puede ser menor, adicionalmente tampoco se tienen en cuenta las perdidas de presión por accesorios y cambios de sección lo que puede llevar a la disminución de la entalpia de los estados presentados, sin embargo la versatilidad del software permite realizar un correcto análisis de la mecánica de fluidos para tasar correctamente este tipo de perdidas. La mecánica computacional utilizada corresponde a una herramienta pedagógica significativa que le permite al estudiante agilizar procesos matemáticos y realizar cálculos para la producción energética de manera mas eficiente además de desarrollar competencias transversales en lenguajes de programación especializados y dedicados exclusivamente a los análisis termodinámicos energéticos.

1) Trabajos futuros y derivados del proyecto de investigación.

Este artículo deriva de la propuesta del CIP de sistemas termodinámicos avanzados aplicados en los diferentes ciclos y sistemas de refrigeración, los resultados de investigación derivaron en diferentes proyectos enfocados a la producción energética y a la conciencia ambiental incrementando tanto la eficiencia térmica de los ciclos termodinámicos como los coeficientes de operación de los ciclos de refrigeración, esto con el objetivo de parametrizar de manera adecuada los diseños de ingeniería, apoyados con herramientas tecnológicas, el estudio energético también sentó un precedente en el análisis de diferentes energías alternativas en el departamento de Nariño como la energía geotérmica en fuentes hiper entálpicas del volcán Cumbal además de un estudio de la energía del viento como capítulo del libro del candidato a doctor Favio Nicolas Rosero, donde se analizan las diferentes condiciones del viento como fuente de producción sostenible en materia de energía.

REFERENCIAS

[1] Y. O. Fernández, L. A. V. Fernández, E. G. Suarez, D. A. Villegas, J. N. Gamboa, y T. I. L. Echevarria, “Gestión del conocimiento y tecnologías de la información y comunicación (TICs) en estudiantes de ingeniería mecánica,” *Apuntes Universitarios*, vol. 10, no. 1, pp. 77–88, 2020. Available: DOI: 10.17162/au.v10i1.419

[2] V. H. Medina-Matute, L. E. Solorzano-Villegas, C. A. Medina-Jiménez, y D. G. V. P. Dimas, “Innovación Educativa para la Enseñanza de la Matemática en Ingeniería,” *Rev. Cient. Arbitrada Investig. Comun., Mkt. y Empresa REICOMUNICAR*, vol. 7, no. 13 Ed. esp., pp. 2–12, 2024. Available: https://reicomunicar.org/index.php/reicomunicar/article/view/219

[3] D. Mosquera-González, A. Valencia-Arias, M. Benjumea-Arias, y L. Palacios-Moya, “Factores asociados al uso de tecnologías de la información y la comunicación (TIC) en los procesos de aprendizaje de estudiantes de ingeniería,” *Formación Universitaria*, vol. 14, no. 2, pp. 121–132, 2021. Available: DOI: 10.4067/S0718-50062021000200121.

[4] N. J. Hernández-Fernández, L. Zumalacárregui-de Cárdenas, y O. Pérez-Ones, "Simulación de condiciones de operación y fluidos de trabajo para ciclos Rankine orgánicos," *Rev. Investig. Desarro. Innov.*, vol. 10, no. 2, pp. 349–358, 2020. Available: https://doi.org/10.19053/20278306.v10.n2.2020.10213.

[5] S. A. Vásquez, A. P. Barturén, y F. M. Carbajal, "Aplicación del simulador Aspen HYSYS en la resolución de problemas del ciclo Rankine regenerativo con recalentamiento intermedio," *Inf. Tecnol.*, vol. 31, no. 3, pp. 199–208, 2020. Available: http://dx.doi.org/10.4067/S0718-07642020000300199.

[6] Y. A. Çengel y M. A. Boles, *Thermodynamics: An Engineering Approach*, 9th ed. New York: McGraw-Hill Education, 2021.

[7] M. A. Ortega Sarceda, *Optimización de la eficiencia de una planta de potencia solar con ciclo Rankine orgánico*, 2022. Available: http://hdl.handle.net/2183/31764

[8] J. Smith y A. Brown, "Enhancing the efficiency of Rankine cycle with reheat: A review," *Int. J. Energy Res.*, vol. 44, no. 3, pp. 1234–1250, 2020.

[9] R. C. Olivera, J. J. M. Cosgalla, y F. D. Sánchez, "Los métodos experimentales y su importancia en la enseñanza de la ingeniería mecánica como complemento al diseño asistido por computadora," 2021.

[10] L. Johnson y T. Williams, "Impact of reheat on the performance of Rankine cycle: A case study," *Appl. Therm. Eng.*, vol. 150, pp. 250–260, 2019.

[11] N. Zobeiry y K. D. Humfeld, "A physics-informed machine learning approach for solving heat transfer equation in

advanced manufacturing and engineering applications," *Eng. Appl. Artif. Intell.*, vol. 101, Art. no. 104232, 2021. Available: https://doi.org/10.1016/j.engappai.2021.104232

[12] J. D. Sánchez Más, *Modelización con el software Engineering Equation Solver (EES) para la optimización de una central térmica de un ciclo real de turbina de vapor utilizado en la central nuclear de Cofrentes*, 2016.

Diego Alejandro Narváez Meza: Mechanical Engineer graduated from the Technological University of Pereira, with a Master's degree in University Teaching from the University of Nariño. He is a tenured professor in the Faculty of Engineering at the Universidad Autónoma de Nariño, teaching in both the Mechanical Engineering and Electronic Engineering programs. He is a member of the Latin American Network of Research Seedbeds, project director, and coordinator of the CIP for advanced systems applied to the thermo-physical model. He also serves as a consultant for the development of qualified registrations for engineering programs, is a member of the undergraduate project evaluation committee, and a technical advisor focused on research areas such as machine design, industrial equipment—where he has supervised technological development projects including prototypes of agro-industrial machines, materials engineering research with a patent in process, and thermodynamic analyses of steam and refrigeration cycles for cogeneration—and the capacity for science, technology, and innovation in endogenous territorial development. He previously worked as a full-time teacher in the area of natural sciences, teaching physics at the Colegio del Sagrado Corazón de Jesús Bethlemitas in Pasto, where he also served as coordinator of the Natural Sciences and Environmental Education department. He is currently a full-time professor in the Faculty of Engineering at the Universidad Mariana, in the Systems Engineering program, where he supervises undergraduate projects as an advisor. He is also an honorary member of the academic-scientific committee of *Tecno Science* journal, serving as an external reviewer.
ORCID: https://orcid.org/0000-0002-9236-6450

Implementation of ANFIS +NN and nature-inspired optimization algorithms for solar radiation prediction.

Implementación de ANFIS + NN y algoritmos inspirados en la naturaleza para predicción de radiación solar.

E. D. Obando-Paredes ; Z. V. Burbano Vallejo ; C. A. Ramírez ; L. C. Revelo Tovar

DOI: https://doi.org/10.22517/23447214.25682
Scientific and technological research paper

***Abstract*- This article presents a hybrid model that makes use of ANFIS (adaptive neuro-diffuse inference system) hybridized with Neural Networks (NN) and optimized with algorithms that are based on natural behaviors, in this case, ant colony (ACO). The model is designed to predict primary resources in a particular region subject to the planning and installation of distributed photovoltaic (PV) generation. The solar primary resource depends on the climatic conditions of the region to be evaluated, and its high variability in short periods presents a challenge in planning energy resources that use variable sources in the long term. In this article, the behavior of a hybrid ANFIS+NN+ACO model is designed, developed, evaluated, and validated. The methodology that is based on data analysis is detailed. First, work is done on climatic databases, which give guidelines for preprocessing and cleaning. Secondly, the climatic variables that predict solar radiation are established. The ANFIS membership functions are then based on the data to capture nonlinearity and extract relationships with predictors. Neural networks support the membership function optimization process, and finally, the optimizer refines and evaluates the response. The response is evaluated using metrics that demonstrate the robustness of the model when capturing and processing data. The study contributes to making visible tools and alternatives to determine energy potentials in climatic regions subject to the future for distributed generation.**

***Keywords*- ANFIS; Fuzzy Systems; Neural Networks; Optimization Algorithms; Solar Radiation Prediction.**

***Resumen*— Este artículo presenta un modelo híbrido que utiliza ANFIS (sistema de inferencia neurodifusa adaptativa) hibridado con redes neuronales (NN) y optimizado con algoritmos basados en comportamientos naturales, en este caso, colonias de hormigas (ACO). El modelo está diseñado para predecir los recursos primarios en una región específica, sujeta a la planificación e instalación de generación fotovoltaica (FV) distribuida. El recurso solar primario depende de las condiciones climáticas de la región a evaluar, y su alta variabilidad en períodos cortos representa un desafío en la planificación de recursos energéticos que utilizan fuentes variables a largo plazo. En este artículo, se diseña, desarrolla, evalúa y valida el comportamiento de un modelo híbrido ANFIS+NN+ACO. Se detalla la metodología basada en el análisis de datos. En primer lugar, se trabaja con bases de datos climáticas, que proporcionan pautas para el preprocesamiento y la limpieza. En segundo lugar, se establecen las variables climáticas que predicen la radiación solar. Las funciones de pertenencia de ANFIS se basan en los datos para capturar la no linealidad y extraer relaciones con los predictores. Las redes neuronales respaldan el proceso de optimización de la función de pertenencia y, finalmente, el optimizador refina y evalúa la respuesta. Esta se evalúa mediante métricas que demuestran la robustez del modelo al capturar y procesar datos. El estudio contribuye a visibilizar herramientas y alternativas para determinar el potencial energético en regiones climáticas sujetas al futuro de la generación distribuida.**

***Palabras clave*—ANFIS; Sistemas Difusos; Redes Neuronales; Algoritmos de Optimización; Predicción de la Radiación Solar**

I. INTRODUCTION.

Accurate solar radiation prediction is critical for managing and optimizing solar energy systems and is essential for sustainable development and reducing carbon emissions [1]. Solar radiation, which depends on various meteorological factors such as atmospheric pressure, clarity index, wind speed, and precipitation, is crucial in planning solar photovoltaic (PV) energy production [2].

Traditional forecasting methods, such as deterministic and statistical models, have shown limitations in handling the complexity and nonlinearity of weather data [3]. Climate nonlinearity, lack of complex data, and variable prediction horizons make traditional models increasingly challenging. In this context, artificial intelligence (AI) systems have emerged as powerful tools to improve the accuracy of solar radiation predictions [4].

This manuscript was submitted on August 14, 2024. Accepted on May 06, 2025. And published on June 30, 2025. This work was supported by the Cooperative University of Colombia, Pasto Colombia.

Obando Paredes. Edgar Dario, EnergIA research hotbed, Cooperative University of Colombia, Pasto Colombia (e-mail: Edgar.obandop@campusucc.edu.co).

Burbano Vallejo. Zarella Valentina Group, research hotbed, Cooperative University of Colombia, Pasto Colombia (e-mail:Zarella.burbano@campusucc.edu.co).

Ramírez, Carlos Alonso is Group, research hotbed, Cooperative University of Colombia, Pasto Colombia (e-mail: carlos.ramirez@campusucc.edu.co).

Revelo Tovar, Luis Carlos is Group, research hotbed, Cooperative University of Colombia, Pasto Colombia (e-mail: luis.revelot@campusucc.edu.co).

Neural networks (NN), support vector machines (SVM), and Fuzzy Logic perform better when considering traditional techniques. However, new trends in research propose hybridization between AI algorithms and nature-inspired optimizers to address the issue of prediction with better results [5], [6].

Among the methods used, the Adaptive Neuro-Fuzzy Inference System (ANFIS) is a technique that integrates the advantages of artificial neural networks (ANNs) and fuzzy logic systems to model complex and nonlinear problems. ANFIS has been successfully used in various prediction and control applications due to its ability to learn from data and handle uncertainty [7], [8], [9]. However, the effectiveness of ANFIS is highly dependent on the proper selection of its input parameters and characteristics. Nature-inspired optimization algorithms, such as Ant Colony Optimization Algorithms (ACOs), offer a robust approach to finding optimal solutions in complex search spaces. ACO has been widely used in optimization problems because it can efficiently explore the search space and adapt to different scenarios. [10], [11]

In this study, we propose a hybrid approach that combines ANFIS with ACO for solar radiation prediction. This approach seeks to optimize the parameters and input characteristics of ANFIS using ACO to improve the accuracy of predictions. The meteorological data used in this study includes variables such as atmospheric pressure, clarity index, wind speed, and precipitation. Given the country's climatic variability, the model is applied to a city in Colombia. Section 2 shows a review of the literature and works related to the application of hybrid models for primary resource prediction. Section 3 presents the methodology for developing the model. Section 4 shows the application and results of the model and, finally, the conclusions. With this work, we aim to overcome the limitations of traditional methods and offer a more accurate and efficient tool for predicting solar radiation.

II. LITERATURE REVIEW

Optimization algorithms are widely used in primary resource quantification, prediction, and the energy industry [12]. The concepts of fuzzy logic and neural networks are combined in the adaptive neuro-fuzzy inference system (ANFIS), an artificial intelligence system [13]. Complex systems that behave nonlinearly and uncertainly may be modeled using ANFIS. Fuzzification, inference engines, and defuzzification are the three essential components of any fuzzy system [14]. The human expert in fuzzy systems obtains fuzzy rules. Fuzzy systems were enhanced with artificial neural networks to use learning algorithms to gather the knowledge of human experts. The neuro-fuzzy system is the name of this link (ANN to fuzzy system) [5].

Much research has been done to evaluate the ANFIS model concerning solar radiation. The work focused on applying the ANFIS model to identify the essential factors that may scatter solar energy. To analyze the impact of such predictions, as stated in Kerman City, the research relied on 10 essential factors. According to the study's results, the length of sunlight is crucial since it impacts how solar radiation diffuses. The mix of sunlight, horizontal global solar radiation, and extraterrestrial solar radiation are crucial factors. The subjects of similar research were the relevance of horizontal sun radiation and the location of interest in affecting thermal or photovoltaic systems. The research aimed to maximize the essential ANFIS model inputs, such as air temperature, month, day, relative humidity, longitude, latitude, and wind speed. The results provide evidence for the influence of global horizontal irradiance on solar radiation and the growth of such systems. Discuss the current state of research on diffuse irradiance and evaluate three reliable machine learning models using almost eight years of hourly observations from Almeria, Spain. The authors suggest that future machine learning models can benefit from advanced optimization techniques, such as evolutionary algorithms and nature-inspired optimization, which can fine-tune the models' parameters and improve their performance on a given dataset. The study compares different types of machine learning models and finds that hybrid models show promise in predicting diffuse fractions. The authors recommend further exploration of hybrid and ensemble models to address gaps in current research.[5], [14], [15], [16]

In work, hybrid models and a standalone adaptive neuro-fuzzy inference system have been created to estimate monthly global solar radiation from various meteorological indicators, such as sunlight duration and air temperature. The findings demonstrated that the hybrid models created had the most dependable and precise estimating capabilities and are thought to be the most effective way of forecasting global solar radiation for diverse purposes [17].

According to this, the SVM approach was used to apply the strategy for attaining the clearness index using the performance metrics for the ANFSI model. It was clear that the ANFSI model and the photovoltaic systems performed better because of the alien solar radiation. Considering this, it is reasonable to use this to estimate solar system radiation [7]. The study [5] discussed the model's importance in correctly forecasting solar diffuse fraction. Following a discussion of the status of diffuse irradiance research, three reliable machine learning (ML) models are tested against a large dataset (spanning over eight years) of hourly observations from Almeria, Spain. The ANFIS model, the multilayer perceptron (MLP), and the hybrid multilayer perceptron grey wolf optimizer (MLP-GWO) were all used in the research. The results showed that the ANFIS model performed better when calculating solar diffuse percentage and was effective.

The ANFIS [18], the adaptive system, and the standard solar radiation prediction model were contrasted. The goal was to comprehend the adaptive system's relevance as a precise and accurate model for calculating and forecasting solar radiation. This worked well since it demonstrated the value of the ANFIS model in increasing solar radiation efficiency.

Some more advanced empirical models can be used to forecast solar radiation. However, this work aims to evaluate the efficiency and dependability of the ANFIS model. It was simpler to connect the meteorological parameters with the present change in duration values for the sunlight and temperature using data from the Hunan province in China, situated in a subtropical monsoon climatic zone. Intriguingly, a model's alteration might affect how accurately a prediction is made; other researchers utilizing the ANFIS model are interested in implementing this [19].

The work uses air temperature to forecast solar radiation. Consistency in air temperature was crucial for solar energy gathering in the North Dakota experiment. The ANFIS model was crucial in establishing the ideal air temperature for optimizing solar energy harvesting worldwide, even though they could have chosen any number of models to analyze the performance accuracy of solar energy harvesting. The results showed that applying the ANFIS model increased the prediction accuracy when using the temperature alone to estimate solar radiation. As a result, it demonstrated its advantages and the necessity of applying it to North Dakota and other places with comparable climatic and meteorological characteristics. A novel intelligence model by fusing the Adaptive Neuro-Fuzzy Inference System (ANFIS) with two metaheuristic optimization algorithms, Salp Swarm Algorithm and Grasshopper Optimization Algorithm, to predict the global solar radiation at various locations in North Dakota, USA. The findings suggest the potential of boosting prediction accuracy by integrating ANFIS with metaheuristic optimization methods [20]. The work conducted a study to predict monthly solar radiation for semi-arid, dry, and wet regions. To estimate solar radiation, they utilized several models, including the multilayer perceptron, radial basis function neural network, and adaptive neuro-fuzzy interface system (ANFIS). The Grasshopper algorithm was utilized to improve the performance of the ANFIS, RBFNN, and MLP models. Three Iranian stations, namely Rasht (with a humid climate), Yazd (with a semi-arid climate), and Tehran (with a slightly arid environment), were used as case studies. The results revealed that relative humidity, wind speed, rainfall, and temperature were these locations' most influential input variables.

The study's primary contribution is the development of innovative hybrid ANFIS models for forecasting monthly solar radiation in various locations [21]. To estimate the daily global solar radiation in Iraq using several metrological properties, the work developed multiple linear regression (MLR) and numerous other AI models, including ANFIS. According to the findings, the results provided by ANFIS are more accurate than those from other prediction models [22]

TABLE I.
REPRESENTATIVE WORKS IN THE USE OF OPTIMIZATION ALGORITHMS INSPIRED BY NATURE+ANFIS.

References	Case study	Input parameters	Output parameter	AI model	Optimization algorithm	Data scale	Research remark	Other if you find appropriately	Performance metrics
[23]	Kerman Iran	Daily diffuse solar radiation on a horizontal surface, global solar radiation on a horizontal surface, sun shine duration, minimum air temperature, maximum air temperature, average air temperature, relative humidity, and water vapor pressure, as well as the calculated values of daily maximum possible sunshine duration, solar declination angle and extraterrestrial solar radiation on a horizontal surface.	Horizontal diffuse solar radiation	ANFIS	-	Daily	The literature does not research the selection of the most crucial variables for predicting diffuse solar radiation well. This study (ANFIS) selects the essential elements impacting horizontal diffuse solar radiation using the adaptive neuro-fuzzy inference method.	The findings indicated that considering the most relevant combinations of two or three ideal inputs offers a compromise between ease of use and high accuracy.	MAPE, MABE, RMSE and R,
[24]	Iran	Global solar radiation in terms of month, day, average air temperature, maximum air temperature, minimum air temperature, air pressure, relative humidity, wind speed, top-of-atmosphere insolation, latitude and longitude	predict the daily global solar radiation	(GMDH) type neural network (MLFFNN) ANFIS	ANFIS-PSO ANFIS-GA ANFIS-ACO	Daily	The findings showed that the GMDH model beats the other produced models even though all studied models can accurately estimate the global horizontal irradiance.	This research has been done to evaluate and compare the accuracy of six artificial intelligence systems since it is crucial to comprehend the availability of solar Energy and the lack of monitoring stations in particular regions.	RMSE, MSE, R2,
[25]	Malaysia	Global solar radiation, including s sunshine duration S (h), and air temperature	Monthly Global Solar Radiation	ANFIS	ANFIS- PSO, ANFIS-GA and ANFIS-DE	Monthly	The importance of this study stems from the need for more precise measurements of solar radiation that may be employed in various applications across a range of sectors, in addition to the measured meteorological parameters that are now accessible.	The results show how effectively ANFIS predicts the level of solar radiation globally and how well it may be used with other soft computing methods.	Clearness index
[26]	Yucatan Peninsula, Mexico	measured meteorological variables: minimum and	predicting daily horizontal	-	ANFIS, SVM, and ANN	Daily	The evaluation shows that the SVM technique performs better than the other techniques. This suggests that the SVM	According to the study's findings, using SVM improves the precision of forecasting global solar radiation in tropical	RMSE, MAE, and R2

		maximum air temperatures, rainfall, and global solar radiation	global solar radiation				technique may offer a promising alternative to the conventional methods for predicting solar radiation.	warm and humid regions such as Mexico's Yucatán, particularly when rainfall is factored into the equation.	
[27]	Almeria, Spain	Global Irradiance, Beam Irradiance, Sunshine Duration Index, (Global/Extraterrestrial-Clearance Index), (Diuse/Extraterrestrial)	Solar (Global/Diuse-Diuse Fraction) (DF)	ANFIS, MLP,	MLP-GWO	Hourly	The results demonstrated that the MLP-GWO model performed better in the training and testing processes, followed by the ANFIS model.	Subsequent investigations ought to employ more advanced hybrid machine-learning techniques. Through hybridization, machine learning models have become more effective and precise. As a result, upcoming models could significantly benefit from tailored evolutionary algorithms and nature-inspired optimization methods to enhance their parameters and scrutinize their algorithmic influence on the quality control of a particular dataset.	MAE, ME, and RMSE
[28]	10 different cities worldwide	Latitude, longitude, minimum and maximum temperatures (°C), relative humidity (%), wind speed (m/s), surface pressure (kPa), amount of air pollutants (O3, NO2, PM2.5, PM10), dew frost point, wet bulb temperature (°C) and mean solar radiation (MJ/m2 /day) on a horizontal surface	Mean monthly global solar radiation	ANN and ANFIS	GA-ANN	Daily	Based on the number of statistical indices specified in this study, the offered model is roughly more formidable in accuracy and credibility than other models created by other researchers.	It may also be expensive or impossible to objectively measure global solar radiation in certain locations since it requires specific equipment. The authors consequently recommend replacing the empirical approach with artificial intelligence to anticipate mean monthly global solar radiation while accounting for input factors in light of the modeling results, particularly the ANFIS method.	RSME= 5.90E−05 , R2 = 0.999, ASM = 5.50E−04, EBM = 0.425
[29]	China	Daily sunshine duration (S), relative humidity (RH), precipitation (Pre), air pressure (AP), daily mean/maximum/minimum temperature (DT/Tmax/Tmin)	Daily global solar irradiance (Hg)	ANFIS, E-IBCM, IYHM		Daily	The findings show that the enhanced empirical models (E-IBCM and IYHM) are more accurate than the original models and that the ANFIS model is more accurate in predicting Hg than the E-IBCM and IYHM models.	The ANFIS model offers the highest accuracy in calculating daily global solar irradiance in China compared to the other E-IBCM and IYHM models. Our future work will enhance the ANFIS model with additional methodologies and combine more diverse input factors to increase modeling accuracy.	RMSE and MAE
[30]	North Dakota, USA	maximum, mean, and minimum air temperature	Solar radiation	ANFIS	ANFIS-SSA, ANFIS-GOA	Daily	The most intriguing finding is that almost every prior SR prediction model was created	It can be claimed that the performance of the hybridized ANFIS-muSG model proved	RMSE. At Baker, Beach, Cando, Crary, and Fingal

					(ANFIS-muSG)		using a variety of parameters. However, the model suggested in this research was built using temperature, and it performed well with an R2 in the range of 0.769 to 0.802.	the muSG algorithm's usefulness for enhancing ANFIS parameters when just one predictor (in this instance, air temperature) is used. This demonstrates the possibility of the proposed method being extensively used for accurate SR prediction.	stations, respectively, the ANFIS-muSG demonstrated a prediction boost compared to the conventional ANFIS model by 42.2%, 32.6, 54.8%, 25.7%, and 49.0% in terms of RMSE.
[31]	Three stations in Iran, namely Rasht (humid climate), Yazd (semi-arid) and Tehran (slightly arid),	relative humidity, wind speed, rainfall, and temperature	monthly solar radiation	ANFIS, RBFNN, MLP	GOA, PSO, SSA	Monthly	The primary contribution of the research is the development of novel hybrid ANFIS models for monthly solar radiation forecasting in various regions.	Future researchers may simultaneously choose the best input combinations and seek the optimal model parameter values using multi-objective optimization methods. Furthermore, prediction models, climatic scenarios, and climate models may be used to forecast solar estimates for the future. Utilizing solar Energy for electricity generation in the future may assist decision-makers.	mean absolute error (MAE), RMSE, NSE, P BIAS
[32]	Iranian city of Tabass	by day of the year (day) as the only input	Estimating the horizontal global solar radiation	an intelligent optimization scheme based upon the adaptive neuro-fuzzy inference system (ANFIS)		Daily	The survey's findings strongly supported using ANFIS to calculate daily worldwide horizontal sun radiation using just $n_{day.}$	There are two benefits to basing global solar radiation predictions on the day of the year. First, there is no reliance on any input component, such as weather information. Additionally, no pre-calculation analysis is required.	Bias error (BE) ranges from –3 to 3 MJ/m2, mean absolute percentage error (MAPE) = 3.9569%, mean absolute bias error (MABE) = 0.6911 MJ/m2, root mean square error = 0.8917 MJ/m2 (RMSE), and correlation coefficient (R) = 0.9908.
[33]	Iraq	daily meteorological data of maximum temperature, minimum temperature, mean temperature, relative humidity, and wind speed	Daily Global Solar Radiation	Artificial Neural Network, adaptive neuro-fuzzy inference		Daily	The study's findings confirmed that the ensemble techniques may improve the performance of single models in the training, validation, and testing processes by up to 19.19%, 7.59%, and 16.81%, respectively.	It might be proposed that additional AI-based models, like SVM, must be used in future research and that their outputs be incorporated in ensemble modeling in light of the study's findings,	Determination coefficient (DC or Nash–Sutcliffe efficiency criterion) and root mean square error (RMSE)

				systems, Meza–Varas, Hargreaves–Samani, and Chen, multi-linear regression (MLR) model				demonstrating that more diverse inputs for ensemble modeling can result in better overall outcomes.	

A. SURVEY ASSESSMENT

According to research by and, the adaptive neuro-fuzzy inference system (ANFIS) model is crucial for accurately forecasting solar radiation. There has always been interest in employing renewable energy to solve the issues of resource depletion and the need for renewable energies [34]. The ANFIS model demonstrates that solar radiation may be forecasted accurately utilizing a variety of factors and suggested performance criteria, including the correlation coefficient, root mean square error, mean absolute percentage error and mean absolute bias error. These are all crucial in evaluating the accuracy of solar radiation and the steps to minimize any inaccuracies that could occur [20]

The results are compared with earlier research conducted in several places throughout the globe to offer a fair evaluation of the chosen ANFIS-muSG model in solar radiation prediction. In this respect, a fair evaluation is carried out to confirm the efficacy of the chosen model in forecasting solar radiation. Notably, in contrast to other research in the literature, the suggested ANFIS-muSG model study attained the desired accuracy. The most intriguing finding is that almost every prior model for predicting solar radiation was built using a variety of inputs. However, the model suggested that the research was building temperature and performed well with an $R[20]^2$ between 0.769 and 0.802.

One of the most effective modeling methods for AI models is the Adaptive Neuro-Fuzzy Inference System (ANFIS), which combines ANN and FL methodologies. According to many studies, ANFIS is more accurate in estimating solar radiation.[3]

For instance, a station in Kuala Terengganu, Malaysia, employed a conventional and hybrid ANFIS model to forecast monthly global solar radiation using several metrological characteristics, such as maximum and lowest air temperature, rainfall, clearness index, and sunlight duration. This model integrated ANFIS with genetic algorithms, particle swarm optimization, and differential evolution methods. Results indicate that the hybrid ANFIS-PSA model predicts solar radiation better than the other models. According to the findings, the results provided by ANFIS are more accurate than those from other prediction models.[17]

Due to its capacity to capture the uncertainty associated with time series data, a comparison of several AI models for solar radiation prediction found that ANFIS is best for solar radiation modeling. However, tuning ANFIS hyperparameters, such as optimizing membership function parameters, is the main issue with this approach. As a result, in earlier research, the classic ANFIS model was hybridized with other optimization techniques to enhance its performance. Although the performance of the current hybrid ANFIS model is promising, it is still necessary to improve the prediction capabilities, given the significance of the precision required in solar radiation measurement. In addition, one of the main drawbacks of current solar radiation prediction models is the need for various input variables that are not always accessible in certain places owing to a lack of monitoring infrastructure.[35]

III. METHODOLOGY OF THE MODEL.

A. DATA TO USE IN THE MODEL.

Various databases and variables are used in resource quantification-prediction in solar primary resource models. According to [36], databases should have features such as:

- Geographical location
- Prediction Horizon
- Co-dependent variables of solar radiation.
- Geographical mesh.

Detailed meteorological data was used to develop and validate the hybrid ANFIS model optimized with ACO, covering multiple variables that directly influence solar radiation. This dataset includes daily atmospheric pressure measurements, clarity index, wind speed, and precipitation collected from reliable weather stations in strategically selected locations.

Atmospheric pressure is a crucial variable that affects air density and, consequently, the amount of solar radiation that passes through the atmosphere. Variations in atmospheric pressure can influence the scattering and absorption of solar radiation. The clarity index is a dimensionless measure representing the fraction of diffuse global solar radiation. This index is critical for understanding the ratio of direct to diffuse radiation, which is essential for modeling the availability of solar Energy under different atmospheric conditions. Wind speed, measured in meters per second (m/s), can affect the scattering of clouds and aerosols in the atmosphere, altering the amount of solar radiation that reaches the Earth's surface. In addition, strong wind conditions are often associated with weather systems that can reduce direct solar radiation. Precipitation, measured in millimeters (mm), indicates the presence of clouds and storm systems that block solar radiation. Periods of high precipitation generally correspond to conditions of low solar radiation due to dense cloud cover.[37]

The data used in this study were obtained from weather stations such as those provided by NASA POWER DAVE V2.0.5 weather services. According to technical documentation, each station provides highly accurate data updated and maintained to rigorous quality standards. Before using the data in the model, a preprocessing process was carried out to ensure its quality and consistency. This process included the elimination of outliers, identifying and eliminating values significantly outside the normal ranges, and using statistical techniques such as percentile analysis and standard deviation. Missing data were imputed using advanced methods such as interpolation, minimizing bias and loss of information. All variables were normalized to a standard scale to ensure that machine learning algorithms can effectively handle differences in variable scales. The typology to develop the model is shown below [38].

B. TYPOLOGY TO BE USED IN THE HYBRID MODEL

The model typology used in this study combines an Adaptive Neuro-Fuzzy Inference System (ANFIS) with Neural Networks (NN) and an Ant Colony Algorithm (ACO) [19], [39]. This combination is chosen due to ANFIS's ability to model complex nonlinear systems, NN's effectiveness in finding optimal solutions in large and complex search spaces, and ACO's robustness in parameter optimization.

ANFIS is a hybrid model that integrates the advantages of neural networks and fuzzy logic systems. Its structure is based on a network of five layers, each of which plays a crucial role in the inference process [39]

1. **Input Layer:** Receives inputs from the system (in this case, weather variables such as pressure, clarity index, wind speed, and precipitation).
2. **Fuzzification Layer**: Transform inputs into fuzzy values using membership features.
3. **Rules Layer**: Applies the fuzzy rules that represent the expert knowledge of the system.
4. **Normalization Layer**: Normalizes the fuzzy values resulting from the rules.
5. **Output Layer**: Generates the system's output using a set of inference functions.

ANFIS is trained using a supervised learning process that adjusts the parameters of membership functions and fuzzy rules using optimization algorithms. This allows it to capture the nonlinear relationships between input and output variables [7].

The neural network (NN) is a computational model inspired by the workings of the human brain. This algorithm can learn complex patterns from data by optimizing their weights and biases through backpropagation processes [40], [41]. The NN optimizes the parameters of the ANFIS model and selects the most relevant features from the dataset. The NN process includes the following steps:

1. **Initialization**: It starts with a defined neural network structure and establishes random initial weights.
2. **Forward propagation**: The input data is propagated through the network, calculating activations at each layer until it reaches the output.
3. **Error calculation**: The error between the output predicted by the network and the actual values is calculated using a loss function, such as mean square error (MSE).
4. **Backpropagation**: The error propagates backward through the network, adjusting weights and biases to minimize the error.
5. **Optimization**: The iterative process continues until a stopping criterion is reached, such as a maximum number of iterations or a convergence in error reduction.

The Ant Colony Algorithm (ACO) is an optimization algorithm inspired by the behavior of ants in foraging. This algorithm is characterized by its ability to find optimal graph paths using pheromones, which are chemical substances that ants deposit to mark effective routes. ACO is used to optimize the parameters of the ANFIS model and select the most relevant features from the dataset [42]. The implementation of the ANFIS+NN+ACO hybrid model follows the following steps:

1. **Data Preprocessing:** Weather data is preprocessed to remove outliers, impute missing data, and normalize variables.
2. **Initial ANFIS Training**: An initial ANFIS model is trained using the full features of the dataset.
3. **Optimization with NN**: NN is used to adjust ANFIS parameters and select the most relevant features, iteratively improving the model's accuracy.
4. **Optimization with ACO**: ACO is used to fine-tune the parameters of the NN-optimized model and select the most relevant features, iteratively further improving the model's accuracy.
5. **Model Evaluation**: The optimized model is evaluated using a validation set to measure its performance in terms of mean square error (MSE) and other relevant metrics [39].

This typology combines the learning and adaptability of ANFIS with the robustness of NN and ACO in parameter optimization, providing a powerful and efficient approach to solar radiation prediction. The integration of these techniques makes it possible to capture the inherent complexity of weather data and significantly improve the accuracy of predictions. Below is the application in a particular region and the model results.

IV. APPLICATION AND RESULTS OF THE MODEL

A. DATA USED IN THE MODEL.

The data used in this study contains meteorological data relevant to the prediction of solar radiation from 1-01-2020 to 20-07-2024. The city chosen is Pasto, located in southwestern Colombia (Latitude 1°12'52.48"N ·Longitude 77°16'41.22" W). This dataset includes six key variables, as shown in Table 2

.

TABLE II. PHYSICAL VARIABLES USED IN THE DATABASE- SOURCES: AUTHORS.

Variable Name	Physical Variable	Units	Min Value	Max Value	Variable Type
PS	Atmospheric pressure	kPa	0.0016	101.40	
WS10M	Wind speed at 10 meters	M/s	0.00	12.20	
T2M	Temperature at 2 meters	°C	-16.60	41.60	Predictor
QV2M	Humidity at 2 meters	g/kg	0.0027	24.20	
RIGHT CORR	Corrected precipitation	mm/hour	0.00	63.70	
CLRSKY_SFC_SW_DWN	Surface radiation	Wh/m^2	0.00	1268.57	Target Variable

The preliminary analysis of the predictors shows that the data are in good condition. The distributions of the variables indicate variability and diversity in the meteorological conditions captured. As shown in Figure 1, the variables do not have anomalous data and high variability is not shown in a few periods, which influences the quality of the model results. The climate predictors that act as input to the model

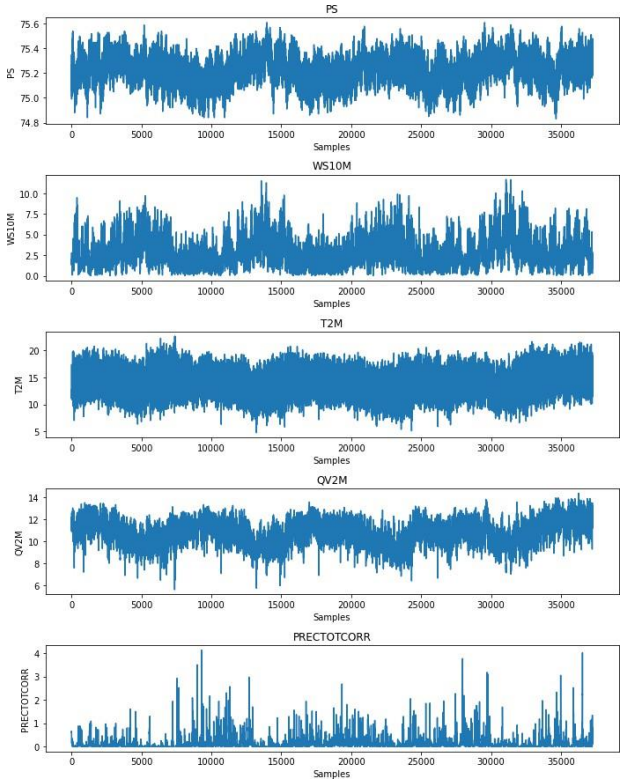

Fig 1. Predictors used in the ANFIS+NN+ACO model. Source: Authors

Figure 2 shows solar radiation in Pasto, the primary resource in the region, which shows high variability. The region's high variability suggests the presence of cloudiness patterns over time and fluctuations in the clarity of the sky, an essential variable in solar PV power generation planning. In addition, seasonal patterns must be captured and predicted by the model.

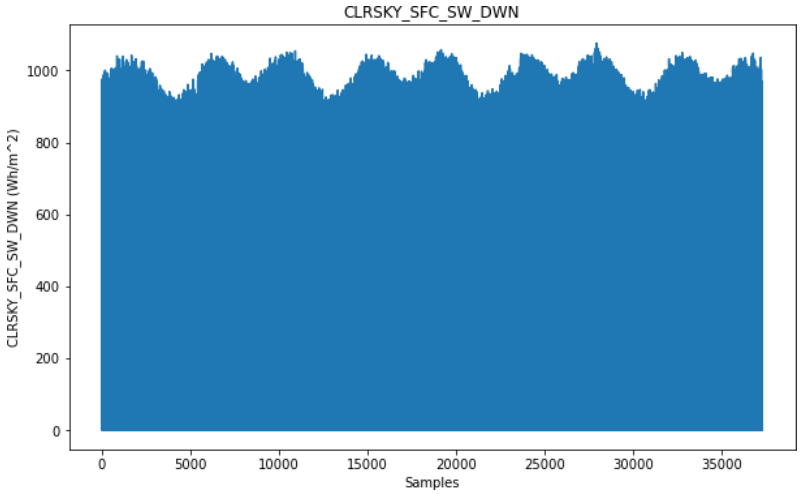

Fig 2. Solar radiation of the particular region in the period. Source: Authors.

B. APPLICATION OF THE MODEL

Figure 3 shows the model's design. The preprocessing and data cleansing stages are responsible for looking for anomalous data or null values that the dataset may have to have continuous inputs to the model. Subsequently, the dataset is normalized to have the predictor variables in the same range. Finally, the dataset is mixed so that the model can capture nonlinearity without redundancy.

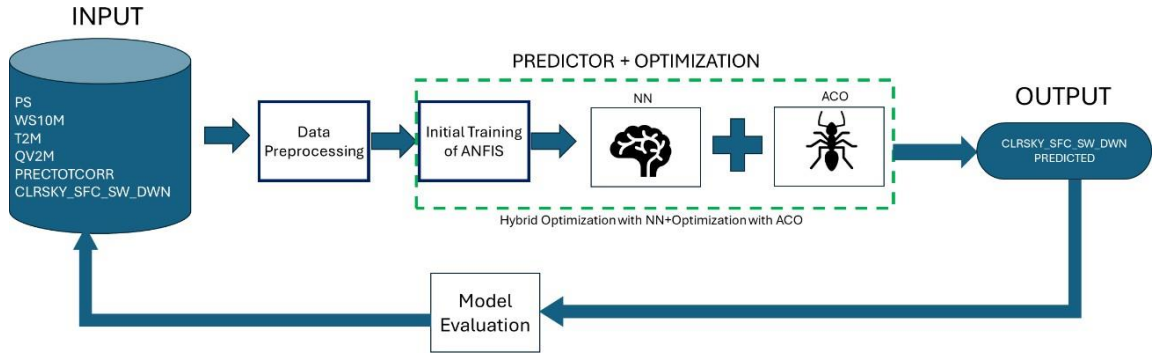

Fig 3. ANFIS+NN+ACO Predictor Model Schema. Own source.

The prediction stage consists of the **ANFIS predictor** first. In its initial training stage, Gaussian membership functions are defined to model the input variables. The inputs are then transformed into fuzzy values using the built-in Fuzzification engine. Then, by applying rules based on fuzzy logic, relationships are established between the input and output variables. Finally, the output of this predictor is the initial training with parameter adjustment of memory functions and fuzzy rules employing a supervised learning algorithm. From a mathematical point of view, ANFIS takes each input variable. $x_i(i = 1,2,3, \dots, n)$ defines the fuzzy membership functions, where being Gaussian, we have as in Equation (1):

$$\mu A_j(x_i) = exp\left(-\frac{(x_i - c_j)^2}{2\sigma_j^2}\right) \qquad (1)$$

Where $\mu A_j(x_i)$, is the degree of membership of the function of membership, is the center of the function, and is the standard deviation.$x_i A_j c_j \sigma_j$

For each Fuzzy rule R_j

R_j: $if\ x_1\ is\ A_{1j}\ and\ x_2\ is\ A_{2j}\ and \dots and\ x_n\ is\ A_{nj}, then\ y_j = a_j x_1 + b_j x_2 + \cdots + z_j x_n$

The weight of the ruler is calculated as shown in Equation 2:

$$w_j = \prod_{i=1}^{n} \mu A_j(x_i) \qquad (2)$$

Finally, the output of the ANFIS model, defuzzification, is calculated as shown in Equation 3:

$$y = \frac{\sum_{j=1}^{m} w_j y_j}{\sum_{j=1}^{m} w_j} \qquad (3)$$

Where m, is the number of rules.

The **neural network and ACO** stages optimize the response of the ANFIS model. With forward typology and hidden layer, the neural network compares the predicted output of ANFIS with the actual values, employing a loss function that adjusts the weights and biases of the network to minimize error. The process is repeated until a stopping criterion is reached, which is the convergence in reducing error for this study. Layers of neurons represent the optimization neural network. For a layered network, the output of the layer is shown in Equation 4:

$$a^l = f(W^l a^{l-1}) + b^l \qquad (4)$$

Where

$a^0 = X$ Network Input
W These are the weights and biases of the layer b^l l
f is the activation function, in this case, sigmoid

The training process adjusts weights and biases to minimize the loss function J, as indicated by Equation 5:

$$J(\theta) = \left(\frac{1}{m}\right) \sum_{i=1}^{m} (h_\theta(x^i) - y^i)^2 \quad (5)$$

The ants in ACO build a solution by moving through the graph and choosing paths based on the probability determined by the number of pheromones and the local heuristic. The pheromones are updated according to the quality of the solutions found by the ants, reinforcing the paths that lead to better solutions. The integration of ACOs for feature selection optimizes the model's parameters, and finally, in the results stage, the performance against standardized metrics is evaluated.

It starts with a population of ants and establishes an initial level of pheromones in the paths of the graph. Each solution is built by moving across the graph and choosing probability-based paths, as shown in Equation 6, which are determined by the number of pheromones and the local heuristic. $\tau_{ij}\eta_{ij}$.

$$P_{ij} = \frac{\tau_{ij}^{\alpha}\eta_{ij}^{\beta}}{\sum_{k\,callowed} \tau_{ij}^{\alpha}\eta_{ij}^{\beta}} \quad (6)$$

where are parameters that control the influence of pheromone and heuristics, respectively α, β

The pheromones are updated according to the quality of the solutions found by the ants, reinforcing the pathways that lead to better solutions, as shown in Equation 7:

$$\tau_{ij} = (1-\rho)\tau_{ij} + \sum_{ant\ k} \Delta\tau_{ij}^{k} \quad (7)$$

Where is the rate of pheromone evaporation, and is the amount of pheromone deposited by the ant.$\rho\Delta\tau_{ij}^{k}k$

The results are then described, and the model is validated.

C. RESULTS AND VALIDATION OF THE MODEL

Figure 4 shows the results of the primary resource prediction. The ANFIS +NN+ACO model performs well. The membership functions implemented in the model, of Gaussian type, can consolidate a solid base of prediction based on fuzzification processes. In addition, the linguistic rules used cover all the spectra found in the cleaning and characterization part of the dataset. The configuration of 64 input layer neural networks and 48 hidden layer neural networks can take resource variations and predictors. By implementing optimization functions represented in Nested and Loss ACOs, the model can capture and respond to the nonlinearity of climate resources.

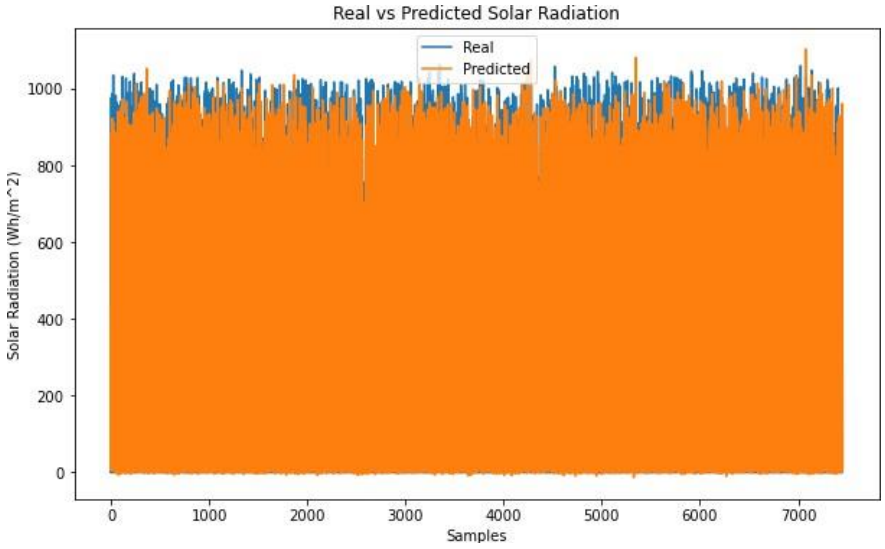

Fig 4. Measured solar radiation vs. predicted solar radiation. Source: Authors

Figure 5 shows the evolution of the data during the model's training and validation stages over 200 epochs. The portion of data used to train-validate the model has a ratio of 70-30. The curves in the graph decrease rapidly at first and then stabilize, suggesting that the model is learning effectively and shows no signs of significant overfitting. The generalization of the model represented by the loss of validation, which is slightly more significant than the training loss, suggests that the model is robust.

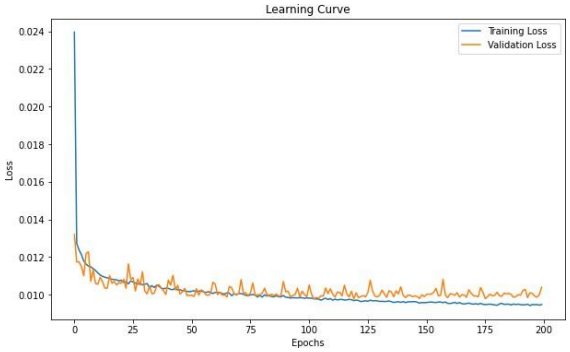

Fig 5. Learning curve of the ANFIS +NN+ACO model. Source: Authors.

Regarding the metrics analysis, shown in Table 3, the MSE (Mean Square Error) indicates that the mean square error between the predicted and actual values is low, suggesting strengths in the model's performance. The RMSE (Root Mean Square Error) makes interpreting the error in the units more accessible. The MAE (Mean Absolute Error) shows that, on average, the model's predictions are 3.07 units away from the actual solar radiation values, which is a relatively low error. Finally, the correlation coefficient indicates that the model explains approximately 91% of the variability of solar radiation data. The metric results are pretty explicit in determining that the model has strengths and can capture the high nonlinearity of the region's data.Wh/m^2R^2

TABLE III. MODEL PERFORMANCE EVALUATION METRICS. FUETNE AUTORES.

Metric	**Value**
MSE	12.818108
RMSE	3.5023
R^2	0.912214

V. FUTURE RESEARCH.

Future researchers may simultaneously choose the best input combinations and seek the optimal model parameter values using multi-objective optimization methods. Furthermore, prediction models, climatic scenarios, and climate models may be used to forecast solar estimates for the future. Utilizing solar Energy for electricity generation in the future may assist decision-makers.

To estimate global sun radiation at various places in North Dakota, USA, Tao et al. (2021) suggested a unique intelligence model by fusing two metaheuristic optimization algorithms with the Adaptive Neuro-Fuzzy Inference System (ANFIS). The study's findings showed that by properly optimizing ANFIS parameters, solar radiation forecast capacity may be increased. The models used in this work can only estimate solar radiation from readily accessible temperatures (maximum, mean, and lowest) in any place. Such less resource-intensive models are crucial for underdeveloped nations with limited access to meteorological information besides rainfall and temperature. The ANFIS-muSG model created in the Tao et al. (2021) research may thus be used for energy harvesting and monitoring in various geographical areas. However, future research may assess how well the model performs when additional meteorological factors include wind speed, cloud cover, sunlight, humidity, and rainfall (Tao et al., 2021).

Additionally, data from satellite remote sensing may be used as an input to enhance model performance in solar radiation forecasting. Using an ensemble strategy, the performance of the hybridized ANFIS-muSG model might be significantly enhanced. In addition, additional cutting-edge optimization methods like quantum-behaved PSO and the Firefly Algorithm may be used to choose input predictors that have been proven successful in model input selection. Empirical mode composition and wavelet transform could also be additional data analysis methods.

VI. CONCLUSIONS

This work presented the design and development of an ANFIS+NN+ACO model. The latter is representative of nature and is an inspiration in data-driven model optimizers. The model is robust in predicting primary solar resources in a particular region. ANFIS settings can be managed so that different strategies are considered in membership functions that can provide greater modeling capacity for nonlinear data. Parameter optimization using ACO is a process of trial and error to determine the best combination(s) for the totalized model. Finally, hybridizing ANFIS with other models, such as neural networks (NN), can leverage the strengths of both approaches, where ANFIS handles uncertainty and fuzzy logic, and NN captures the complex nonlinear relationships, thus achieving greater accuracy in predictions. However, several limitations must be acknowledged. First, the model relies on the availability and quality of meteorological data, which may be limited in some regions. Second, although the model was trained and tested using data from a specific geographic area (Pasto, Colombia), its generalization capability to other climatic zones remains to be validated. Third, the computational cost of hybrid models that include metaheuristic optimization can be relatively high, especially for large datasets or longer prediction horizons. Finally, the current model does not incorporate satellite-based inputs or multi-objective optimization, which could further enhance its accuracy and adaptability.

Despite these limitations, the hybrid ANFIS+NN+ACO model provides a strong framework for evaluating solar energy potential and supporting the planning of distributed generation

systems. Future work should address these constraints by incorporating diverse geographic datasets, reducing computational load, and integrating additional optimization strategies to improve generalizability and scalability.

Models of this nature are essential inputs to quantify the solar potentials of regions subject to distributed generation installation with variable primary resources.

ACKNOWLEDGMENT

The authors thank the project Development of a multi-agent transactional model of non-conventional Energy for the department of Nariño, Pasto BPIN 2021000100499.

I. REFERENCES

[1] F. O. Hocaoğlu, "Stochastic approach for daily solar radiation modeling," *Solar Energy*, vol. 85, no. 2, pp. 278–287, 2011, doi: 10.1016/j.solener.2010.12.003.

[2] E. Obando-Paredes and R. Vargas-Cañas, "Desempeño de un sistema fotovoltaico autónomo frente a condiciones medioambientales de una región en particular," *Rev Acad Colomb Cienc Exactas Fis Nat*, vol. 40, no. 154, pp. 27–33, 2016, doi: 10.18257/raccefyn.301.

[3] Z. M. Yaseen *et al.*, "Implementation of Univariate Paradigm for Streamflow Simulation Using Hybrid Data-Driven Model: Case Study in Tropical Region," *IEEE Access*, vol. 7, pp. 74471–74481, 2019, doi: 10.1109/ACCESS.2019.2920916.

[4] E. D. Obando, S. X. Carvajal, and J. Pineda, "Solar radiation prediction using machine learning techniques: a review," *IEEE Latin America Transactions*, vol. 17, no. 4, pp. 684–697, 2019.

[5] R. Claywell, L. Nadai, I. Felde, S. Ardabili, and A. Mosavi, "Adaptive neuro-fuzzy inference system and a multilayer perceptron model trained with grey wolf optimizer for predicting solar diffuse fraction," *Entropy*, vol. 22, no. 11, pp. 1–14, Nov. 2020, doi: 10.3390/e22111192.

[6] M. Sharafi and T. Y. ElMekkawy, "Stochastic optimization of hybrid renewable energy systems using sampling average method," Dec. 01, 2015, *Elsevier Ltd*. doi: 10.1016/j.rser.2015.08.010.

[7] V. H. Quej, J. Almorox, J. A. Arnaldo, and L. Saito, "ANFIS, SVM and ANN soft-computing techniques to estimate daily global solar radiation in a warm sub-humid environment," *J Atmos Sol Terr Phys*, vol. 155, pp. 62–70, Mar. 2017, doi: 10.1016/j.jastp.2017.02.002.

[8] H. Ishibuchi and Y. Nojima, "Analysis of interpretability-accuracy tradeoff of fuzzy systems by multiobjective fuzzy genetics-based machine learning," *International Journal of Approximate Reasoning*, vol. 44, no. 1, pp. 4–31, 2007, doi: 10.1016/j.ijar.2006.01.004.

[9] C. Bergmeir and M. Ben, "frbs : Fuzzy Rule-Based Systems for Classification," *J Stat Softw*, vol. 65, no. 6, pp. 1–30, 2015, doi: 10.18637/jss.v069.i12.

[10] H. Ghazvinian *et al.*, "Integrated support vector regression and an improved particle swarm optimization-based model for solar radiation prediction," *PLoS One*, vol. 14, no. 5, May 2019, doi: 10.1371/journal.pone.0217634.

[11] M. Restrepo, C. A. Cañizares, J. W. Simpson-Porco, P. Su, and J. Taruc, "Optimization- and Rule-based Energy Management Systems at the Canadian Renewable Energy Laboratory microgrid facility," *Appl Energy*, vol. 290, no. October 2020, 2021, doi: 10.1016/j.apenergy.2021.116760.

[12] E. Obando-Paredes, "Algoritmos genéticos y PSO aplicados a un problema de generación distribuida . PSO and genetic algorithms applied to a distributed generation problem," vol. 22, no. 1, pp. 15–23, 2017, doi: https://doi.org/10.22517/23447214.14301.

[13] E. Group, "FUZZY ALGORITHM FOR ESTIMATION OF SOLAR IRRADIATION," vol. 63, no. 1, pp. 39–49, 1998.

[14] A. Khosravi, R. O. Nunes, M. E. H. Assad, and L. Machado, "Comparison of artificial intelligence methods in estimation of daily global solar radiation," *J Clean Prod*, vol. 194, pp. 342–358, Sep. 2018, doi: 10.1016/j.jclepro.2018.05.147.

[15] B. Mohammadi and Z. Aghashariatmadari, "Estimation of solar radiation using neighboring stations through hybrid support vector regression boosted by Krill Herd algorithm," *Arabian Journal of Geosciences*, vol. 13, no. 10, May 2020, doi: 10.1007/s12517-020-05355-1.

[16] K. Mohammadi, S. Shamshirband, C. W. Tong, K. A. Alam, and D. Petković, "Potential of adaptive neuro-fuzzy system for prediction of daily global solar radiation by day of the year," *Energy Convers Manag*, vol. 93, pp. 406–413, Mar. 2015, doi: 10.1016/j.enconman.2015.01.021.

[17] L. M. Halabi, S. Mekhilef, and M. Hossain, "Performance evaluation of hybrid adaptive neuro-fuzzy inference system models for predicting monthly global solar radiation," *Appl Energy*, vol. 213, pp. 247–261, Mar. 2018, doi: 10.1016/j.apenergy.2018.01.035.

[18] S. Riahi, E. Abedini, M. Vakili, and M. Riahi, "Providing an accurate global model for monthly solar radiation forecasting using artificial intelligence based on air quality index and meteorological data of different cities worldwide", doi: 10.1007/s11356-021-14126-8/Published.

[19] L. Zou, L. Wang, L. Xia, A. Lin, B. Hu, and H. Zhu, "Prediction and comparison of solar radiation using improved empirical models and Adaptive Neuro-Fuzzy Inference Systems," *Renew Energy*, vol. 106, pp. 343–353, 2017, doi: 10.1016/j.renene.2017.01.042.

[20] H. Tao *et al.*, "Global solar radiation prediction over North Dakota using air temperature: Development of novel hybrid intelligence model," *Energy Reports*, vol. 7, pp. 136–157, Nov. 2021, doi: 10.1016/j.egyr.2020.11.033.

[21] H. Huang, S. S. Band, H. Karami, M. Ehteram, K. wing Chau, and Q. Zhang, "Solar radiation prediction using improved soft computing models for semi-arid, slightly-arid and humid climates," *Alexandria Engineering*

Journal, vol. 61, no. 12, pp. 10631–10657, Dec. 2022, doi: 10.1016/j.aej.2022.03.078.

[22] V. Nourani, G. Elkiran, J. Abdullahi, and A. Tahsin, "Multi-region Modeling of Daily Global Solar Radiation with Artificial Intelligence Ensemble," *Natural Resources Research*, vol. 28, no. 4, pp. 1217–1238, Oct. 2019, doi: 10.1007/s11053-018-09450-9.

[23] Mohammadi, Kasra, S. Shamshirband, D. Petković, and H. Khorasanizadeh, "Determining the most important variables for diffuse solar radiation prediction using adaptive neuro-fuzzy methodology; Case study: City of Kerman, Iran," *Renewable and Sustainable Energy Reviews*, vol. 53, pp. 1570–1579, 2016, doi: 10.1016/j.rser.2015.09.028.

[24] A. Khosravi, R. O. Nunes, M. E. H. Assad, and L. Machado, "Comparison of artificial intelligence methods in estimation of daily global solar radiation," *J Clean Prod*, vol. 194, pp. 342–358, 2018, doi: 10.1016/j.jclepro.2018.05.147.

[25] L. M. Halabi, S. Mekhilef, and M. Hossain, "Performance evaluation of hybrid adaptive neuro-fuzzy inference system models for predicting monthly global solar radiation," *Appl Energy*, vol. 213, no. November 2017, pp. 247–261, 2018, doi: 10.1016/j.apenergy.2018.01.035.

[26] V. H. Quej, J. Almorox, J. A. Arnaldo, and L. Saito, "ANFIS, SVM and ANN soft-computing techniques to estimate daily global solar radiation in a warm sub-humid environment," *J Atmos Sol Terr Phys*, vol. 155, no. February, pp. 62–70, 2017, doi: 10.1016/j.jastp.2017.02.002.

[27] R. Claywell, L. Nadai, I. Felde, and S. Ardabili, "Adaptive Neuro-Fuzzy Inference System and a Multilayer Perceptron Model Trained with GreyWolf Optimizer for Predicting Solar Di use Fraction," *Entropy*, vol. 22, no. 1192, 2020.

[28] S. Riahi, E. Abedini, M. Vakili, and M. Riahi, "Providing an accurate global model for monthly solar radiation forecasting using artificial intelligence based on air quality index and meteorological data of different cities worldwide," *Environmental Science and Pollution Research*, vol. 28, no. 36, pp. 49697–49724, 2021, doi: 10.1007/s11356-021-14126-8.

[29] L. Zou, L. Wang, L. Xia, A. Lin, B. Hu, and H. Zhu, "Prediction and comparison of solar radiation using improved empirical models and Adaptive Neuro-Fuzzy Inference Systems," *Renew Energy*, vol. 106, pp. 343–353, 2017, doi: 10.1016/j.renene.2017.01.042.

[30] H. Tao *et al.*, "Global solar radiation prediction over North Dakota using air temperature: Development of novel hybrid intelligence model," *Energy Reports*, vol. 7, pp. 136–157, 2021, doi: 10.1016/j.egyr.2020.11.033.

[31] H. Huang, S. S. Band, H. Karami, M. Ehteram, K. wing Chau, and Q. Zhang, "Solar radiation prediction using improved soft computing models for semi-arid, slightly-arid and humid climates," *Alexandria Engineering Journal*, vol. 61, no. 12, pp. 10631–10657, 2022, doi: 10.1016/j.aej.2022.03.078.

[32] Mohammadi, Kasra, S. Shamshirband, C. W. Tong, K. A. Alam, and D. Petković, "Potential of adaptive neuro-fuzzy system for prediction of daily global solar radiation by day of the year," *Energy Convers Manag*, vol. 93, pp. 406–413, 2015, doi: 10.1016/j.enconman.2015.01.021.

[33] V. Nourani, G. Elkiran, J. Abdullahi, and A. Tahsin, "Multi-region Modeling of Daily Global Solar Radiation with Artificial Intelligence Ensemble," *Natural Resources Research*, vol. 28, no. 4, pp. 1217–1238, 2019, doi: 10.1007/s11053-018-09450-9.

[34] K. Mohammadi, S. Shamshirband, D. Petković, and H. Khorasanizadeh, "Determining the most important variables for diffuse solar radiation prediction using adaptive neuro-fuzzy methodology; Case study: City of Kerman, Iran," Jan. 01, 2016, *Elsevier Ltd*. doi: 10.1016/j.rser.2015.09.028.

[35] O. Castillo and P. Melin, "Optimization of type-2 fuzzy systems based on bio-inspired methods: A concise review," *Inf Sci (N Y)*, vol. 205, pp. 1–19, Nov. 2012, doi: 10.1016/j.ins.2012.04.003.

[36] M. Sengupta *et al.*, "Best Practices Handbook for the Collection and Use of Solar Resource Data for Solar Energy Applications.," *Technical Report - NREL/TP-5D00-63112*, no. February, pp. 1–255, 2015, doi: 10.1016/j.solener.2003.12.003.

[37] C. Voyant *et al.*, "Machine learning methods for solar radiation forecasting: A review," 2017, *Elsevier Ltd*. doi: 10.1016/j.renene.2016.12.095.

[38] NASA, " Prediction of Worldwide Energy Resource (POWER) ."

[39] S. A. Pérez-Rodríguez *et al.*, "Metaheuristic Algorithms for Solar Radiation Prediction: A Systematic Analysis", doi: 10.1109/ACCESS.2017.DOI.

[40] A. I. Galushkin, *Neural Networks Theory*. 2007.

[41] L. Ma, N. Yorino, and K. Khorasani, "Solar radiation (insolation) forecasting using constructive neural networks," *Proceedings of the International Joint Conference on Neural Networks*, vol. 2016-Octob, no. 3, pp. 4991–4998, 2016, doi: 10.1109/IJCNN.2016.7727857.

[42] S. S. Screening *et al.*, "Solar resource assessment and site evaluation using remote sensing methods," *Fraunhofer ISE*, vol. 1, no. February, p. 162, 2015, doi: Fraunhofer ISE.

Edgar Dario Obando is a Physical Engineer from the Universidad del Cauca and holds a Master's degree in Electrical Engineering from the Universidad Nacional de Colombia. He currently works as a professor at the Universidad Cooperativa de Colombia, where he has been recognized for his outstanding teaching performance. His research interests include energy systems, machine learning, Big Data, and solar radiation prediction, with several scientific publications focused on metaheuristic techniques, photovoltaic systems, and artificial intelligence applications in energy resources. ORCID: https://orcid.org/0000-0002-2515-7640.

Burbano-Vallejo Zarella, Sixth semester Software Engineering student at the Universidad Cooperativa Campus Pasto. I belong to the ESLINGA Semillero EnergIA research group. I have completed a diploma in coding and programming at the Universidad Pontificia Javeriana. ORCID: https://orcid.org/0009-0000-6559-9980

Ramirez, Carlos Alonso, Master in Environmental Engineering from the Mariana University of Pasto. Specialist in Finance from the University of Valle Cali. Industrial Engineer from the National University of Colombia, Manizales. Research Professor from the Cooperative University of Colombia - UCC Pasto. Research topics: Alternative energies and industrial production systems. ORCID: https://orcid.org/0000-0002-3559-6225

Revelo Tovar, Luis Carlos, Systems engineer with emphasis on software from the Antonio Nariño University, with specialization in marketing management from the Jorge Tadeo Lozano University and systems auditing from the Antonio Nariño University, master's degree in free software from the Autonomous University of Bucaramanga. With experience in software development, software project management, computer networks and software architecture in public and private entities. ORCID: https://orcid.org/0009-0001-0990-9603

Mathematical model for analyzing the fluorescence emission of biological tissue

Modelo matemático para el análisis de la emisión de fluorescencia del tejido biológico

B. Segura Giraldo ; M. Londoño Orozco ; S. G. Chacón Chamorro

DOI: https://doi.org/10.22517/23447214.25544
Scientific and technological research paper

***Abstract*—Optical emission fluorescence spectroscopy allows for determining biochemical changes in healthy and pathological biological tissue, either in vivo or in biopsies. The aim of the study is to analyze the chemical and physical properties of cervical tissue. A mathematical model is presented to examine and observe the fluorescence emission of tissue. During the development of precancerous states, the optical properties of the tissue can be altered not only by the light dispersion and the fluorescence increase in the epithelium but for the fluorescence reduction in the stroma. The Beer-Lambert Law was used to describe light propagation in the tissues. Four components of cervix tissue were identified: collagen, elastin, NADH, and flavins. By applying the developed model, it was possible to characterize each fluorophore present through Gaussian sub-spectra, providing support for the medical diagnosis of precancerous lesions in cervical tissue. The model yielded predictions with a good spectral fit, and the contribution of each fluorophore showing significant differences in the signal parameters, particularly for collagen and NADH.**

***Index Terms*—Detection cancer; Fluorophore; Mathematical Model; Optical Fluorescence Spectroscopy; Precancerous Tissue.**

***Resumen*—La espectroscopía de fluorescencia por emisión óptica permite determinar cambios bioquímicos en tejidos biológicos normales y patológicos, ya sea in vivo o en biopsias. El objetivo de este estudio es analizar las propiedades químicas y físicas del tejido cervical. Se presenta un modelo matemático para examinar y observar la emisión de fluorescencia del tejido. Durante el desarrollo de estados precancerosos, las propiedades ópticas del tejido pueden alterarse no solo por la dispersión de la luz y el aumento de fluorescencia en el epitelio, sino también por la disminución de fluorescencia en el estroma. Para describir la propagación de la luz en los tejidos se utilizó la Ley de Beer-Lambert. Se identificaron cuatro componentes en el tejido cervical: colágeno, elastina, NADH y flavinas. Al aplicar el modelo desarrollado, fue posible caracterizar cada fluoróforo presente mediante subespectros gaussianos, brindando soporte al diagnóstico médico de lesiones precancerosas en el tejido cervical. El modelo arrojó predicciones con un buen ajuste espectral, evidenciando diferencias significativas en los parámetros de señal de cada fluoróforo, especialmente en el caso del colágeno y el NADH.**

This manuscript was submitted on January 25, 2025. Accepted on May 6, 2025. And published on June 30, 2025. Belarmino Segura Giraldo is affiliated with Universidad Nacional de Colombia Sede Manizales, Grupo de Investigación Instrumentación Física, Manizales, Colombia (e-mail: bsegura@unal.edu.co). Mariana Londoño Orozco is affiliated with Universidad Nacional de Colombia Sede Manizales, Grupo de Investigación Instrumentación Física, Manizales, Colombia (e-mail: malondonoor@unal.edu.co) Sofía Geovana Chacón Chamorro is affiliated with Universidad Nacional de Colombia Sede Manizales, Grupo de Investigación Instrumentación Física, Manizales, Colombia (e-mail: sgchacon@unal.edu.co)

***Índice de términos*— Detección de cáncer; Espectroscopia óptica de fluorescencia; fluoróforos; modelo matemático; tejido precanceroso.**

I. INTRODUCTION

CERVIX cancer is the 4th most common cancer in women around the world. Its development is very slow, and it tends to begin with a lesion called cervical intra-epithelial neoplasia (CIN), from which several years can go until it becomes cancer. However, this kind of lesion can be identified in an early stage, and that way, strong actions can be taken to face the illness on time [1]. Early detection of CIN represents a fundamental especially role in the mortality reduction related to cervix cancer, especially during the last 50 years [2]. Opposite of it, nowadays, cervix cancer keeps being a relevant threat to woman's health [1], [2].

For cervix detection, different diagnosis methods have been used such as cytology, HVP molecular detection, and colposcopy [3]. However, the techniques mentioned above are not efficient enough to detect cervix cancer in its early stages, and many times, a histopathological analysis of biopsies is required for the final diagnosis. For example, a sensibility rate of 32 to 90% and 94% of specificity is associated with cytology analysis according to [4], [5] due to the limited number of tests and reading errors. Other diagnosis methods present lower percentages of sensibility and specificity. To improve the variables mentioned above, it is necessary to find other diagnosis methods [5].

An important technique that was used during previous decades to detect cervix pre-cancerous lesions was fluorescence spectroscopy. This technique can offer high sensitivity as well as a specific and accurate diagnosis without extracting the tissue [6], [7]. Even, when there is huge empirical evidence that sensitivity suggests that the mentioned technique can be used to discriminate between normal and dysplastic cervical tissue, there is no wide information to understand the differences in the biological tissue of fluoresce spectrum of normal and dysplastic tissue [8]. The work can be done by developing algorithms to simulate the spectrum.

The aim of this research is to simulate the normal and pathological fluorescence spectrum of cervix tissue by using mathematical models based on the Beer-Lambert law, to study the fluorescence emission of molecules in the tissue such as collagen, elastin, NADH, and flavins. Results are compared with the ones obtained for in-vivo tissue.

II. METHODOLOGY

The following methodology was conducted to conduct the research.

a. Equipment and materials

The system used for the research was composed of an optical fiber probe, a spectrograph, and a computer interface. This equipment was used to record fluorescence spectral data of cervix in-vivo tissue.

Characteristics of laser are:

- Wavelength: 337.1 nm
- Pulse: 5 ns
- Repetition rate: 33 Hz
- Pulsed transmitted energy: 300 µJ

b. Objective Sample

For this research, a pilot test for normal and pathological cervix tissue of 50 patients between 17 and 60 years old was conducted. Patients had previous results of cervical cytology. Informed consent was obtained for each patient and the study was reviewed and approved by specialists of the *IPS-Universidad de Caldas – Unidad de Cáncer de Cuello Uterino y Cáncer de Mama*.

Fluorescence spectra were taken according to the pre-established protocol conducted by experts. Figure 1 shows the cervix and the four points where measurements were done. On each point, 30 spectra were taken, and then, during signal processing, an average spectrum was obtained.

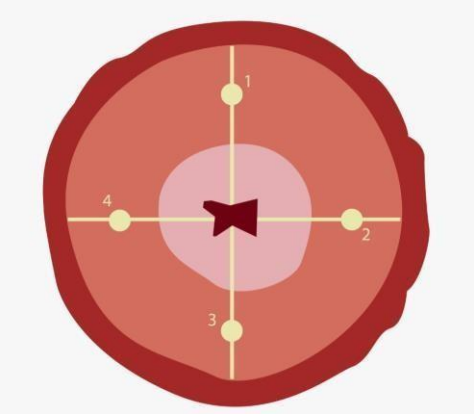

Fig. 1. Sections and points of the cervix to take the spectrum.

III. THEORETICAL FRAME

a. Optical Spectroscopy Fluorescence

Spectroscopy comes from electromagnetic interaction with matter. That produces state transitions for molecules and level transitions for atoms. Transitions can be electronic in the visible spectrum (UV), vibrational in the infrared (IR) or rotational in the radio waves. Spectroscopy relates three processes that are going to be explained in more detail in the following sections: radiation absorption, light emission, and dispersion.

Fluorescence is the ability of certain molecules to absorb energy and emit electromagnetic radiation with different wavelengths. That is why, optical fluorescence spectroscopy is a method to analyze the fluorescence of a sample using a beam of light that can be normally found in the ultraviolet spectral range. Fluorescence is widely used in analytic measurements, and photochemical analysis of biological systems, alimentary products, pharmaceutical products, clinical samples, and scientific research [9], [10].

b. Physics Principles

Spectrophotometric methods are based on the Beer-Lambert Law and are used to analyze various media, including biological tissues. The law defines that the totality of light emitted by a sample can decrease due to the number of absorption materials in its trajectory (concentration), the distance that light must go through (optical path distance), and the probability that the photon in the particular wave amplitude can be absorbed by the material (extinction coefficient) [11].

Lambert-Bourger law is derived from Beer-Lambert law and can be expressed in (1), which relates to the light absorption of an optically diluted homogenous medium and its thickness,

$$\frac{dI}{I} = \mu_a \, dl. \tag{1}$$

Where I represents the intensity, l the distance, μ_a the absorption coefficient and dl is a successive layer of the absorbent medium. Transmitted light intensity through the distance l is described by (2)

$$I = I_0 e^{-\mu a l}, \tag{2}$$

being I_0 the initial light intensity. Another important concept in spectrophotometric theory is the absorption length (inverse of the absorption coefficient) which can be defined as the distance required for the beam of light to decrease in e^{-1} of the initial light intensity. That allows a redefinition of the transmitted light intensity shown in (3)

$$I = I_0 10^{-kl} \tag{3}$$

where k is the extinction coefficient.

In a sample, a radiation beam passes through a solution layer containing a specific absorbent species with defined thickness and concentration. Beam power is attenuated due to the

interaction between photons and absorbent particles, generating absorbance of the solution, which is a fraction of the incident radiation [12] and can be defined as (4)

$$A = kl = log \frac{I_0}{I}. \quad (4)$$

The equation above expresses the quantity of energy emitted that crosses a body in a certain amount of time. Absorbance measure is made in spectrophotometers with the aim of generating an absorption or emission spectrum. The intensity of electromagnetic radiation distribution in terms of wavelength is used to determine the characteristics of the sample [13], [14].

c. *Fluorescence of biological tissue in a single layer*

In 1852, August Beet determined that the absorption coefficient has a linear relation with the concentration of a diluted substance within the medium, represented by its concentration (c) and a constant (α), that is, as presented in (5)

$$\mu_a = \alpha c. \quad (5)$$

From the above, (2) can be rewritten such as (6)

$$I = I_0 e^{-\alpha cl} = I_0 e^{\epsilon cl}. \quad (6)$$

Where ϵ is known as the specific extinction coefficient.

When extending the definition for n substances in a sample, the total absorbance corresponds to the individual sum of the extinction coefficient times their respective concentrations times the distance. This relationship is formulated in Equation (6), which follows the same structure as Equation (7).

$$I = I_0 e^{-(\Sigma_{i=1}^{n} e_i c_i) l}. \quad (7)$$

The analysis of the research is focused on the study of emitted photon energy distribution. That is why, expressing the fluorescence intensity for each absorbed photon in the medium The emission characteristics, in terms of the emitted photon wavelength, are important [15] and can be defined as shown in (8)

$$\int_0^\infty F_\lambda(\lambda F) d\lambda F = \Phi_F \quad (8)$$

where Φ_F is the quantum yield, $F_\lambda(\lambda F)$ is the fluorescence emission spectrum function that reflects the probability distribution of different transition vibratory levels from state S_1 to state S_0. The emission spectrum is characterized by each fluorophore in the biological tissue.

In a practice sense, the fluorescence intensity $I_F(\lambda(F))$ measured at a certain wavelength $\lambda(F)$ is proportional to $F_\lambda(\lambda F)$ and to the number of photons that are absorbed at a excitation wavelength λ_E . It is convenient to replace the number of absorbed photons for the absorption intensity $I_A(\lambda_E)$, which is defined as the difference between intensities of incident $(I_o(\lambda_E))$ and transmitted $(I_T(\lambda_E))$ light. In that sense (9),

$$I_A = I_o(\lambda_E) - I_T(\lambda_F). \quad (9)$$

From the above, fluorescence intensity can be represented like in (10)

$$I_F(\lambda_E, \lambda_F) = kF_\lambda(\lambda_F) I_A(\lambda_E), \quad (10)$$

Then, by using (6), the above expression can be rewritten as (11):

$$I_F(\lambda_E, \lambda_F) = kF_\lambda(\lambda_F) I_0(\lambda_E)(1 - e^{\epsilon(\lambda E) cl}). \quad (11)$$

The factor k depends on several parameters, especially in the visualization optical configuration and the bandwidth of the monochromator.

Measures of the variations of I_F in terms of λ_F, for a set excitation wavelength, reflects the changes in $F_\lambda(\lambda_F)$ and then, provides the fluorescence spectrum.

Equation (11) can be modified to obtain a less complex expression using the expansion of exponential series $1 - e^{\epsilon(\lambda E) cl} = \epsilon(\lambda_E) cl + \frac{(\epsilon(\lambda_E) cl)^2}{2!} + \cdots$, gettingin like (12)

$$I_F(\lambda_E, \lambda_F) = kF_\lambda(\lambda_F) I_0(\lambda_E) \epsilon(\lambda_E) cl. \quad (12)$$

The relation above allows to observe the fluorescence intensity is proportional to the concentration at a low absorbance and then, the linear variation is lost with the absorbance increase. Additionally, when fluorescence spectroscopy is used to make quantitative evaluation of the fluorophore's concentration, the proportionality between fluorescence and concentration intensity, only diluted solution must be taken into account.

IV. RESULTS AND DISCUSSION

The fluorophores from the cervix tissue that contribute to the emission fluorescence signal under light excitation of 337,1 nm are collagen, elastin, NADH and flavins [16]. Figure 2 shows emission and absorption spectrum for each fluorophore in the cervix tissue. Spectrum were obtained from spectroscopy measurements and the following signal processing with gaussian fit. Figure 2a shows absorption spectrum between 200 and 500 nm, and Figure 2b shows emission spectrum between 300 and 600 nm.

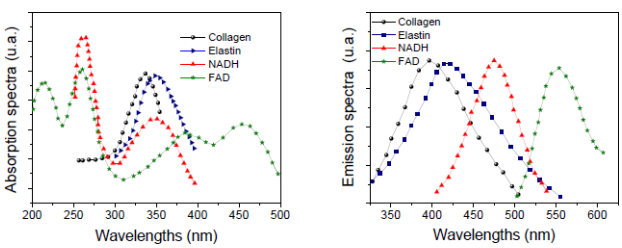

a) Absorption spectrum b) Emission spectrum

Fig. 1. Spectrum with gaussian fit for each fluorophore (collagen, elastin, NADH and flavins) in the cervix tissue.

From the previous spectrum, different statistical and geometrical characteristics were extracted and are shown in Table I. There, λ_{kx} and λ_{km} refer to wavelength in the central absorption and emission spectrum respectively. I_{kx} and I_{km} are the absorption and emission intensities, respectively. W_{kx} and W_{km} corresponds to the width at mid height of each curve in the absorption and emission spectrum, respectively.

TABLE I
EXTRACTED CHARACTERISTICS FROM ABSORPTION AND EMISSION SPECTRUM OF FLUOROPHORES IN THE CERVIX

	Absorption			Emission		
Fluorophore	λ_{kx}	I_{kx}	W_{kx}	λ_{km}	I_{km}	W_{km}
Collagen	336.35	1	34.85	393.85	1	60.69
Elastin	352.03	1	46.40	405.48	1	73.08
NADH 1st peak	262.61	1	25.8	474.28	1	55.42
NADH 2nd peak	345.51	0.45	54.41			
Flavine 1st peak	260.17	1	28.77	557.44	1	65.51
Flavine 2nd peak	387.20	0.45	112.29			
Flavine 3rd peak	457.57	0.5	100.58			

Based on data from Table I, contribution factor for each fluorophore at excitation wavelength ($\lambda_x = 337.1nm$) and emission wavelength ($\lambda_m = 457.8nm$) are extracted and denoted as: CF_{kx} and CF_{km}. Equations (13) and (14) show the expression of the previous values following the definition of Beer-Lambert law.

$$CF_{kx} = I_{kx}\, e^{-2\left(\frac{\lambda x-\lambda_{kx}}{W_{kx}}\right)^2} \quad (13)$$

$$CF_{km} = I_{km} e^{-2\left(\frac{\lambda m-\lambda_{km}}{W_{km}}\right)^2} \quad (14)$$

where k depends on each fluorophore: Collagen: $k = 1$, Elastin: $k = 2$, NADH: $k = 3$, Flavins: $k = 4$.

Combining (7) and (4), total spectrum absorption with fluorophores contribution can be determined by (15) and (16),

$$A_x = \sum_{k=1}^{4} \mu_{ak}\, c_k CF_{kx}\,, \quad (15)$$

$$A_m = \sum_{k=1}^{4} \mu_{ak}\, c_k\, CF_{km}. \quad (16)$$

Where c_k represents the contributions of each fluorophore, which are unknown variables in the model and that should be calculated to contribute to the research of normal and pathological cervical tissue.

Then, total absorbance and transmission in wavelength range of 200 to 700 nm are calculated considering steps of 0.3nm, which fits with the spectrometer resolution used for the in-vivo measures. That way, contribution factors with wavelength function $CF_{k\lambda}$ are calculated

$$CF_{k\lambda} = I_{kx}\, e^{-2\left(\frac{\lambda-\lambda_{kx}}{W_{kx}}\right)^2}. \quad (17)$$

Using the contribution factor, it results that total absorbance and transmittance can be expressed as in (18) and (19),

$$A_\lambda = \sum_{k=1}^{4} \mu_{ak}\, c_k CF_{k\lambda}, \quad (18)$$

$$T_\lambda = 10^{-A}. \quad (19)$$

From those contributions, fluorescence emission intensity (I_m is calculated in (20) due to each fluorophore in the cervix tissue

$$I_{tm} = \sum_{k=1}^{4} I_k\, c_k 10^{-A\lambda} 10^{-Ax} e^{-2\left(\frac{\lambda-\lambda_k}{W_k}\right)^2} - I_{tr}. \quad (20)$$

Where I_k, λ_k, and W_k are intensity, central wavelength, and width at mid high of the emission peaks of each fluorophore from cervix tissue, respectively.

Additionally, I_{rr} shows in (21) is a Raman band dispersion of water and an adjustment variable inside the system

$$I_{tr} = c_{rr}\, I_{rr}\, 10^{-A\lambda} 10^{-Ax} e^{-2\left(\frac{\lambda-\lambda_{rr}}{W_{rr}}\right)^2}. \quad (21)$$

I_{rr}, λ_{rr}, W_{rr}, and c_{rr} are intensity, central wavelength, width at mid height and the contribution to dispersion band, respectively. For obtaining the parameters and their dependencies on fluorophore, each filtered and averaged spectrum was fitted using the mathematical model developed in this research, which simulates the characteristic fluorescence spectrum through (13), (14) y (20). This model is based on a sum of Gaussian bands, each representing the contribution of a specific fluorophore to the processes of absorption, excitation, emission, and transmission described throughout the theoretical development.

The fitting process employs a nonlinear least squares method to extract a set of spectral features from the fluorescence data, including fluorescence intensities, full width at half maximum (FWHM), central wavelengths, and relative contributions of each endogenous fluorophore (such as collagen, elastin, NADH, and flavins) present in the cervical tissue. This procedure is applied individually to each measurement point obtained from the spectral fluorescence data collected on cervical tissue samples. Figure 3 shows the adjustment. The spectrum shows similar shapes that the ones on the literature [17].

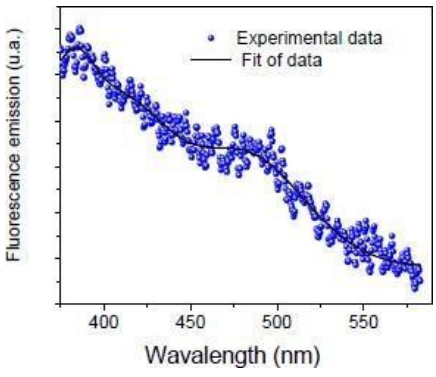

Fig. 3. Original fluorescence spectrum and adjustment with the mathematical model.

The correlation coefficients R and R^2 are calculated as normalized measures of the relationship between the variables representing the filtered and averaged spectrum and the fitted spectrum. Based on these values, the spectra corresponding to analysis points with a correlation index below ***0.9*** are discarded.

Applying the optical fluorescence spectroscopy technique, an initial test was done in normal and pathological cervical tissue of 50 patients between 17 and 60 years old. To obtain the spectrum from spectral tissue information, results from the patient's histopathology were used with the idea to find the range of each category: normal and pathological. As shown in Figure 4, there exist a notable separation between the normal and pathological spectrum, as well as the differences between maximum and minimum intensities.

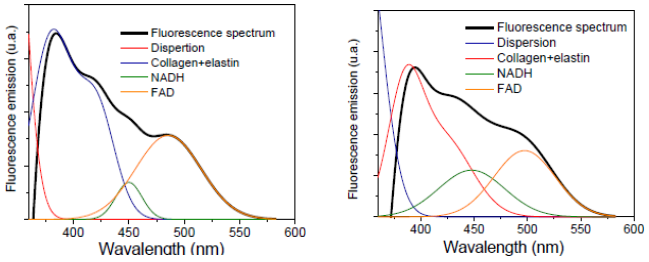

a) Normal spectrum b) Pathological spectrum

Fig. 4. Spectrum with gaussian fit for each fluorophore: collagen, elastin, NADH, and flavins.

Now, Table II shows the results from simulation process using the proposed method, where parameters for Equation 20 are obtained from the patient's previous classification, followed by the classification in normal and pathological, and the extraction of the mean and standard deviation to register I_k, λ_k, W_k, and c_k. It is important to notice that collagen decrease in epithelial cells that preserve the cell structure produce an increase on NADH levels, altering normal homeostasis of the epithelium. Biological changes are analyzed and recognized using fluorescence emission spectroscopy, showing the difference between normal and pathological cervical tissue.

TABLE II
PARAMETERS OBTAINED WITH THE MATHEMATICAL MODEL, MEAN AND STANDARD DEVIATION (SD) FOR NORMAL AND PATHOLOGICAL TISSUE.

		Normal		Pathological	
Parameter	Fluorophore	Mean	SD	Mean	SD
I_k	Collagen	0.613	0.074	0.539	0.068
	Elastin	0.672	0.110	0.586	0.129
	NADH	0.588	0.107	0.542	0.186
	Flavins	0.689	0.174	0.597	0.177
λ_k	Collagen	382.878	3.615	384.530	5.716
	Elastin	417.023	5.489	415.874	6.252
	NADH	459.613	17.847	456.316	17.403
	Flavins	498.730	19.411	500.228	16.989
W_k	Collagen	35.146	10.738	31.765	11.383
	Elastin	47.541	11.877	43.936	17.876
	NADH	47.794	18.571	45.351	17.456
	Flavins	62.418	14.706	58.517	16.521
c_k	Collagen	3.590	1.146	2.537	1.119
	Elastin	3.425	0.975	2.193	0.913
	NADH	5.049	1.896	3.933	1.268
	Flavins	5.785	2.220	4.483	1.983

V. CONCLUSION

Fluorescence spectral information obtained from the technique implementation and the mathematical model developed in the research, suggest that contributions in the cervix tissue such as collagen, elastin, NADH, and flavins. The mathematical model implemented allowed to correlate the fluorophores contributions in each spectrum. In normal tissue, the collagen contribution is higher than the NADH contribution, while in pathological tissue, the NADH contribution is higher than the collagen one. The previous one is a characteristic that makes possible the identification of normal and pathological tissue. There is evidence that the combination of fluorescence spectroscopy with the adjustment model with gaussian decomposition can be an alternative tool to support medical diagnosis and recognition of intraepithelial damage in cervix tissue.

ACKNOWLEDGMENT

The author gratefully acknowledges the financial support of MinCiencias. This work was also helped by the research group of Magnetismo y Materiales Avanzados of Universidad Nacional de Colombia sede Manizales, the group of Cáncer de Cuello Uterino y Cáncer de Mama at Universidad de Caldas and the group Automática at Universidad Autónoma de Manizales.

REFERENCES

[1] K. Duraisamy, "Methods of Detecting Cervical Cancer", *Advances in Biological Research*, vol 4, no 4, pp. 226-232, 2011.
[2] J. Cordero Martínez, "Citologías alteradas y algunos factores de riesgo para el cáncer cervicouterino" *Revista Cubana de Obstetricia y Ginecología*, vol. 41, no. 4, 2015
[3] A. A. Angeleri, "Calidad de la toma exo-cervical en la prevención del cáncer de cuello uterino", *Medicina (Buenos Aires)*, vol. 77, no. 6, pp. 512-514, 2017
[4] M. F. S. Nava, "Certeza diagnóstica de la colposcopia, citología e histología de las lesiones intraepiteliales del cérvix" *Médica Sur*, vol. 20, no. 2, pp. 95-99, 2018.
[5] J. E. Samperio Calderón, "Eficacia de las pruebas diagnósticas del Cáncer Cervicouterino y Virus del Papiloma Humano", *JONNPR*, VOL. 4, NO. 5, PP. 551-566, 2015. DOI: 10.19230/jonnpr.2953
[6] M. A. Corti, "Aplicación de técnicas ópticas sobre tejidos y fluidos corporales para el diagnóstico no invasivo de enfermedades oncológicas", Ph. D. Dissertation, Universidad Nacional de la Plata, 2020.
[7] K. Pandey, "Fluorescence Spectroscopy: A New Approach in Cervical Cancer", *The Journal of Obstetrics and Gynecology of India*, vol 62, pp. 432-436, 2012.
[8] A. Sordillo, "Optical spectral fingerprints of tissue from patients with different breast cancer histologies using a novel fluorescence spectroscopy device", *Technology in cancer research and treatment*, vol. 12, no. 5, pp. 455-461, 2013. Doi: 10.7785/tcrt.2012.500330
[9] L. Escuero, "Principio de fluorescencia", Master's thesis, Universidad Complutense, Facultad de Farmacia, 2018.
[10] I. Tuñón, "Espectroscopia para el estudio de la materia", Universidad de Valencia, Tech. Rep., 2014.
[11] D. Skoog. *Principios de Análisis Instrumental*. ESPAÑA: 5ª. McGraw Hill, 2001.
[12] A. López, "Sistema para mediar la absorbancia (espectrofotómetro)", Master's tesis, Tecnológico Nacional de México, Instituto de Tuxla Gutierrez, 2015.

[13] B. Segura. “Espectroscopía óptica de fluorescencia aplicada al soporte de diagnóstico médico de precánceres de tejido de cuello uterino”, Tesis de Doctorado, Universidad Nacional de Colombia, Departamento de Ingeniería Eléctrica, Electrónica y Computación, 2009.
[14] N. Díaz. “Espectrofotometría: Espectros de absorción y cuantificación colorimétrica de biomoléculas”, Campus Universitario de Rabales, Tech. Rep., 2010.
[15] B. Valeur, *Molecular fluorescence: principles and applications.* John Wiley & Sons, 2012.
[16] K. Vishwanath, “Fluorescence spectroscopy in vivo”. *Encyclopedia of Analytical Chemistry: Applications, Theory and Instrumentation,* 2011. DOI: 10.1002/9780470027318.a0102.pub2
[17] A. Mahadevan, “Study of the fluorescence properties of normal and neoplastic human cervical tissue”, *Lasers in surgery and medicine,* vol. 13, no. 6, pp. 647-655, 1993. DOI: 10.1002/lsm.1900130609

Segura Giraldo, Belarmino is a PhD in Engineering, Master in physics, and Specialist in University Teaching. Professor-researcher at the Universidad Nacional de Colombia Sede Manizales. He supports academic and research processes in the areas of biophysics, physical instrumentation, biomaterials, digital signals, and image processing, among others. He began his work on the fluorescence spectroscopy technique during his PhD studies with population in Caldas. He has been directing and researching on several projects based on the development of low cost and portable equipment for diagnosis support of breast and cervix cancer. Currently, he keeps working on the fluorescence spectroscopy technique, as well as others, with the aim of optimizing the techniques so they can be used in medical the environment. ORCID https://orcid.org/0000-0001-9205-8573.

Londoño Orozco, Mariana is a MSc Physics student at Universidad Nacional de Colombia Sede Manizales. She is a Physicst Engineer and Mathematician. She has worked on biophysics for more than 3 years. She participated in a Young Researcher program from Ministerio de Ciencia, Tecnología e Innovación during 2021-2022 where she contributed to the development of equipment for diagnosis support techniques for breast and cervix cancer. She is currently member of Grupo de Instrumentación Física where she keeps working of the optimization of the techniques and development of in vivo tests. https://orcid.org/0000-0002-3260-5333.

Sofía Chacón is a physical and electronic engineer from the Universidad Nacional de Colombia, Manizales. She holds a master’s degree in electronic engineering from the Universidad de Nariño (Colombia) and is certified in Artificial Intelligence. She worked as a *Joven Investigadora* on a research project focused on cervical cancer detection techniques, where she applied fluorescence optical spectroscopy and mathematical modeling of biological systems. She also served as a research assistant on project which focused on energy transactions for multiple agents. Her main research interests include mathematical modeling of systems, fluorescence optical spectroscopy, energy management systems, optimization in power systems, game theory applications, distributed energy management, and peer-to-peer energy markets. ORCID https://orcid.org/0000-0002-5687-6883.